CFD SIMULATIONS OF FLUIDIZED BED BIOMASS GASIFICATION

A Thesis Submitted to the

National Institute of Technology, Rourkela

In Partial Fulfillment for the Requirements

Of

Master of Technology (Res.) Degree

In

Chemical Engineering

By

Ms. Chinmayee Patra

Roll No. 611CH304

Under the guidance of

Dr. (Mrs.) Abanti Sahoo

Department of Chemical Engineering
National Institute of Technology
Rourkela – 769008

Department of Chemical Engineering
National Institute of Technology
Rourkela – 769008

CERTIFICATE

This is to certify that M.Tech. (Res.) thesis entitled, "**CFD Modelling for Fluidized Bed Biomass Gasification"** submitted by **Ms. Chinmayee Patra** in partial fulfillments for the requirements of the award of Master of Technology (Res.) degree in Chemical Engineering at National Institute of Technology, Rourkela is an authentic work carried out by her under my supervision and guidance. She has fulfilled all the prescribed requirements and the thesis, which is based on candidate's own work, has not been submitted elsewhere.

Date:

Dr. (Mrs.) Abanti Sahoo
Department of Chemical Engineering
National Institute of Technology
Rourkela – 769008, Odisha

ACKNOWLEDGEMENT

First I bow down to pay my heartfelt regards to my God for giving me the health, the patience and his kind blessings which I have received from the beginning to the end of the Master's study. Next, I would like to express my deepest and sincere gratitude to my Supervisors Prof. (Mrs.) Abanti Sahoo for valuable guidance, inspiration, constant encouragement and heartfelt good wishes. Her genuine interest in the research topic, free accessibility for discussion sessions, thoughtful and timely suggestions has been the key source of inspiration for this work. I feel indebted to my supervisor for giving abundant freedom to me for pursuing new ideas.

I am also highly grateful to Prof R. K. Singh, Head of the Department, Chemical Engineering for providing the necessary facilities for the project. I take this opportunity to pay my humble gratitude to the members of my Reaserch Scrutiny Committee Prof. B. Munshi, Prof. H. M Jena of Chemical Engineering Department and Prof. B. B Nayak of Ceramic Engineering Department for their thoughtful advices given during discussion sessions.

I would like to greatly acknowledge and thank the entire Administration and Management of National Institute of Technology, Rourkela, for enabling and supporting me for this work.

I would also like to take this opportunity to give heartily thanks to Ms. Pranati Sahoo, Ms. Subasini Jena, Mr. Debi Prasad Tripathy and Mr. Sambhurisha Mishra for their valuable contributions and moral support towards the success of this work.

Last but definitely not least I would like to owe a deep sense of thankfulness to all my family members particularly to my parents for their much appreciated support, encouragement and good wishes during my studies. They have given me fresh impetus along all my journeys to reach the goal I have been aiming for.

Ms. Chinmayee Patra

Date:

M.Tech (Research)

CONTENTS

LIST OF TABLES

LIST OF FIGURES

NOMENCLATURE

d	Diameter (m)
V	Volume (m^3)
α	Volume Fraction
ρ	Density of Fluid(kg/m^3)
v	Velocity(m/s)
p	Pressure(Pa)
$\bar{\bar{\tau}}$	Stress-strain Tensor (Pa)
$\vec{g}$	Acceleration due to Gravity (m/s^2)
F	Force (N)
μ	Viscosity (kg/m. s)
h	Specific Enthalpy (J/kg)
q	Heat Flux (J)
S_q	Source Term (kg/s)
K_{pq}	Interphase Momentum Co-efficient
K_{Is}	The Fluid-solid and Solid-solid Exchange Coefficient
I_{2D}	Second Invariant of the Deviatoric Stress Tensor (Pa)
τ_p	Particulate Relaxation Time (s)
Re	Reynolds Number
e_{gs}	Coefficient of Restitution

$g_{0,ls}$	Radial Distribution Co-efficient
C_D	Drag Co-efficient ($kg/m^3.s$)
$C_{fr,ls}$	Coefficient of Friction Between the l^{th} and s^{th} Solid Phase Particles
Θ_s	Solid Phase Granular Temperature (m^2/s^2)
g_0	Radial Distribution Function
μ_s	Solid Shear Viscosity (kg/m. s)
$\mu_{s,col}$	Collision Viscosity (kg/m. s)
$\mu_{s,kin}$	Kinetic Viscosity (kg/m. s)
$\mu_{s,fr}$	Frictional Viscosity (kg/m. s)
λ_s	Bulk Viscosity (kg/m. s)
ϕ	Angle of Internal Friction (deg)
K_{Θ_s}	Diffusion Co-efficient(kg/m s)
Υ_{Θ_s}	Collisional Dissipation of Energy (J)
Φ_{ls}	Energy Exchange Between l^{th} Solid Phase and s^{th} solid Phase (J)
η	Rate Exponent
$\vec{U}_q$	Phase-weighted Velocity (m/s)
ε_q	Dissipation Rate (m^{-2}/s^{-3})
$\Pi_{k_q}=\Pi_{\varepsilon_q}$	Influence of Dispersed Phase on Continuous Phase q
$G_{k,q}$	Turbulence Kinetic Energy (m^2/s^2)
$\tau_{F,pq}$	Characteristic Relaxation Time (s)

Γ_{ϕ}	Diffusion Co-efficient For ϕ
∇	Gradient
G_k	Generation of Turbulence Kinetic Energy due to the Mean Velocity Gradients
G_b	Generation of Turbulence Kinetic Energy due to Buoyancy
$C_{i\varepsilon}$	Constants
Y_M	Contribution of the Fluctuating Dilatation in Compressible Turbulence to the Overall Dissipation Rate
σ_k	Turbulent Prandtl Numbers For k
σ_ε	Turbulent Prandtl Numbers For ε
S_k, S_ε	User-defined Source Terms
β	Coefficient of Thermal Expansion
Pr_t	Turbulent Prandtl Number
M	Mash Number
a	Speed of Sound
Y_i	Mass Fraction of Species
N	Total Number of Phases
R	Rate of Reaction
T	Temperature (K)
K	Rate Constant
v'	Stoichiometric coefficient of reactant

v"	stoichiometric coefficient of product

SUBSCRIPTS

j	Species
t	Turbulent
r	Reaction
p, q	Phase
s	Solids

ABBREVIATION

CFD	Computational Fluid Dynamics
FVM	Finite Volume Method
2-D	Two Dimensional
FBG	Fluidized Bed Gasifier
TFM	Two Fluid Models
KTGF	Kinetic Theory Of Granular Fluid Bed
PDE	Partial Differential Equations
GAMBIT	Geometry and Mesh Building Intelligent Toolkit
SIMPLE	Semi-implicit Method for Pressure-linked Equations
CH4	Methane
CO	Carbon Monoxide
CO2	Carbon Dioxide

H2O	Water
Re	Reynolds Number

ABSTRACT

CFD simulation of fluidized bed biomass gasification process has been carried out in the present work. The gas-solid interaction, thermal-flow behavior and gasification process inside a fluidized-bed biomass gasifier are studied using the commercial CFD solver ANSYS/FLUENT13.0. Velocity profile, bed expansion, solid movement, temperature profile, species mass fractions have been focused in the present work. Three phases are used to model the reactor (sand, solid phase for the fuel, and gas phase). All phases are described using an Eulerian approach to model the exchange of mass, energy and momentum. In the present work rice husk is considered as feed material and sand is taken as the inert bed material. The influences of particle properties viz. particle size (530μm, 856μm) and other operating parameters namely, gas velocity (0.05-2 m/s) and temperature (600-1000K) of the gasifier have been investigated comprehensively. It is found that superficial gas velocity has a strong influence on the axial solids velocity and subsequently on the down flow of solids. Gas temperature and species distributions indicate that reactions in the instantaneous gasification model occur very fast and finish very quickly. Temperature of 1000K, superficial velocity of air of 0.7m/s is found to be most favourable for gasification of rice husk with an indication of 100% carbon conversion. On the other hand the reactions in the finite-rate model involve gas-solid reactions which occur slowly with unburnt chars at the exit. The mass fractions of product gas are also validated with the experimental data. Thus the developed simulation model will be a powerful theoretical basis for accurate design of FBG.

CHAPTER ONE

INTRODUCTION

1.1 Energy Demand

Modern world and structure of our society are inextricably related to energy production. Now a days, the global population has become highly dependent on the production of energy through the industrial burning of fossil fuels. However, burning of fossil fuels releases lot of CO_2 which is considered as greenhouse gas into the Earth's atmosphere leading to the global warming. Furthermore, the fossil fuels do not exist in infinite amounts and also their prices are increasing strongly due to their potential shortage in the market. For these reasons, it is need to shift this dependence from fossil fuels to sustainable energy sources. Scarcity of fossil fuels has led towards the use of alternative energy sources like solar, wind, hydro power, geothermal and biomass.

Biomass is a renewable organic matter such as agricultural crops, wood and wood waste, organic components of municipal and industrial wastes, or animal waste which has been utilized for energy production for many years. It is also a viable option for the substitution of coal in industrial combustors and gasifiers as it is a large sustainable energy resource. For reducing harmful emissions, the variation of fuels is not the only solution. Other options include different conversion processes and variation in the technologies carrying out such conversions is also required.

Among the technologies available for using biomass for producing energy, gasification is relatively new which is considered as an environmentally benign solution. Gasification is primarily a thermo-chemical conversion of organic materials at elevated temperature with partial oxidation. With gasification in general, low-value or waste feedstocks such as biomass, municipal waste, refinery residues, petroleum coke and any carbonaceous compounds can be used to produce heat or power with high efficiency. Specifically, biomass gasification is CO_2 neutral. This is because the carbon content of biomass is absorbed by the CO_2 of the atmosphere for which net CO_2 production is zero. The product of gasification is called syngas or product gas (mixture of CO, CH_4 and H_2) which has a high percentage of hydrogen thus syngas is advantageous to all other fuels. All these reasons make biomass gasification a promising alternative for heat and power production.

The concern for climatic variations has triggered the interest in biomass gasification making fluidized bed gasifiers as one of the popular options, occupying nearly 20% of the

market. A fluidized bed reactor (FBR) is a type of device that can be used to carry out a variety of multiphase chemical reactions. Fluidized beds have various industrial uses ranging from fluid catalytic cracking, combustion, gasification, and pyrolysis, to coating processes used in the pharmaceutical industry (Basu, 2006).

1.2 Advantages of Biomass Gasification

In the gasification process the organic matters are converted into fuels known as syngas at high temperature and in a controlled environments in the presence of oxygen. Syngas is a type of an effective fuel. The process of gasification has helped the industry to utilize organic material to generate electricity and helps the industrial plants to reduce their production cost. Gasification was originally developed to produce electricity for small household chores such as for cooking and lighting.

The recent development in the gasification process has drawn the attention of industry to use plastic as a combustion material. The syngas generated in the process of gasification is used to produce electricity and effective mechanical power. As compared to the solid fuels, gaseous fuel is believed to be more environments friendly. The process of gasification does not emit greenhouse gases in the air.

The electric power generated in this process is much cheaper than the steam cycle. The increasing use of this process has also attracted the automobile industry to make cars that can use syngas as a fuel. Now a days the use of gasification is also popular in agriculture. Gasification is a vital process to save the major fertilizer and chemical industry (Basu, 2006).

1.3 Computational Fluid Dynamics

Computational fluid dynamics (CFD) is one of the branches of fluid mechanics that uses numerical methods and algorithms to solve and analyze problems that involve fluid flows. Due to a combination of increased computer efficacy and advanced numerical techniques, the numerical simulation techniques such as CFD becomes a reality and offers an effective means of quantifying the physical and chemical process in the biomass thermo- chemical reactors under various operating conditions within a virtual environment. The results of accurate simulations can help to optimize the system design and operation and understand the dynamic process inside the reactors. CFD modeling techniques are becoming widespread in the biomass thermo chemical conversion areas. Researchers have been using CFD to simulate and analyze the

performance of thermo chemical conversion equipment such as fluidized beds, fixed beds, combustion furnaces, firing boilers, rotating cones and rotary kilns. CFD programs predict not only fluid flow behavior, but also heat and mass transfer, chemical reactions (e.g. devolatilization, combustion), phase changes (e.g. vapour in drying, melting in slagging), and mechanical movement (e.g. rotating cone reactor). Compared to the experimental data, CFD model results are capable of predicting qualitative information and in many cases accurate quantitative information. CFD modeling has established itself as a powerful tool for the development of new ideas and technologies. (Wang et al., 2008)

1.4 Overview of Project Topic

Gasification of biomass is therefore currently considered as a clean and most promising source of energy. It is very difficult and also very much time consuming to get the optimum conditions through experimentations by varying the operating conditions for a fluidized bed gasifier. Sometimes carrying out experiments might not be viable or not be economical at all. Therefore CFD modelling has proven to be a viable option over recent years. With the continual enhancement of computational capabilities, it is capable of carrying out such modifications to determine optimum design and operating conditions before experimental modifications are carried out. Very little literature is found on CFD modelling for FBG. Therefore, in this work it is planned to carry out CFD modelling for the hydrodynamic studies, thermal flow behaviour inside the bed and reaction model of fluidized bed gasifier which will support experimental investigations.

1.5 Objectives of the Present Study

1.5.1 General objective

In order to support experimental investigations, the work presented here is dedicated to the simulation of the laboratory scale bubbling fluidised bed gasifier. The primary objective of this project is to simulate the gasification processes in a fluidised bed using computational fluid dynamics (CFD) modelling which takes into account the different gas-solid behaviours, heat transfers and thermal conversion processes using multiphase flow modelling from the commercial software package ANSYS 13.0. The Eulerian-Eulerian model, or two-fluid model (TFM), is utilized with particle interactions being considered through the incorporation of the kinetic theory of granular flow (KTGF).

1.5.2 Specific objectives

The specific objective of this study is to perform a comprehensive numerical investigation of Fluidized Bed Gasifiers with the specific goals of establishing a robust and reliable computational model for gasification and thereby gaining the understanding of thermal-flow and gasification process. The main objectives of the present work are as follows:

- To model and simulate the hydrodynamic behaviors of fluidized bed gasifier at isothermal condition using rice husk as biomass particle.
- Investigating the thermo-flow behavior inside the gasifier with particles.
- Modelling of the gasification chemical reactions.

1.6 Plan of the Thesis

The present work has been reported in a thesis comprising of seven chapters viz. Introduction, Literature Survey, Computational Flow Model and Numerical Methodology, Modelling of Multiphase Flow, Hydrodynamic Study, Heat and Reaction Model and Conclusion.

Chapter 1 represents the complete introduction to the present study including the energy demand and the potential of biomass as a sustainable alternative energy source. Gasification process along with advantages of biomass gasification and role of computational fluid dynamics are described. The objectives of the present work are also discussed in this chapter.

Chapter 2 deals with literature reviews i.e. the research works which have previously been carried out in the areas of fluidized bed and FBG modelling using computational fluid dynamics approach.

Chapter 3 describes the computational models in details where the numerical methodology adopted in the CFD simulation has been discussed.

Chapter 4 deals with the fundamentals of the Eulerian multiphase models where volume fractions, conservation equations, kinetic theory of granular flows and complementary models are presented to explain the Eulerian approach.

Chapter 5 describes the simulations of bed hydrodynamics for FBG. Various hydrodynamic characteristics of fluidized bed gasifier are studied.

Chapter 6 describes thermal flow behavior within the FBG and reaction models developed for the gasification process with the corresponding result and discussions.

Chapter 7 deals with the overall conclusion for the present work.

CHAPTER TWO

LITERATURE REVIEW

2.1 Gasification

Gasification is a process that converts organic or fossil-based carbonaceous materials into carbon monoxide, hydrogen, carbon dioxide, methane and nitrogen (if air is used as the oxidizing agent). This is achieved by reacting the material at high temperatures with a controlled amount of air, oxygen or steam. It contains a series of steps: drying, devolitisation, char gasification and gas phase reactions. Also, the final product gas composition is a result of important endothermic and exothermic chemical reactions that take place inside the gasifier. The exothermic reactions provide heat to support the endothermic reactions through partial combustion. Eventually a steady state will be reached and the gasifier will maintain its operation at a certain temperature.

The major challenge of gasification technology is to improve quality of the product gas which determines the extent of the post-treatment. Tar formation (complex hydrocarbons CxHy) can put an investment in great risk. Multiphase flow, gas-solid interaction, chemical reactions and turbulence are responsible for the composition of the raw output gas. So far, many empirical models and structures have been developed which fail to optimize the technology and result in industrial-scale units. For this reason, computational fluid dynamic (CFD) simulations are being developed. However, the lack of knowledge in the field of chemical reactions puts a big barrier on the accuracy of the simulation projects.

2.2 Gasifying Mediums

The gasification process requires gasification agent for the thermo chemical conversion of carbonaceous feed stock. oxygen, air, steam or a combination of these is used as the oxidizing agent for the requirement of quality of the product gas.

When the gasifying agent is air, the process is named air gasification and the producer gas has lower quality in terms of heating value due to the high percentage of nitrogen mixed in the gas. This gas is suitable for boilers, engines and turbines.

If the gasifying agent is pure oxygen or steam, it is called oxygen or steam gasification respectively. In this case the producer gas has relatively higher quality and can be used for conversion to methanol and gasoline. In the present study air is taken as gasifying medium.

2.3 Zones of Gasifier

Gasification process is carried out in different stages or zones. Different zones of gasifier are named as follows.

- Drying zone
- Pyrolysis zone
- Oxidation/Combustion zone
- Reduction zone

2.3.1 Drying zone

The main operation in drying zone is the removal of moisture. Biomass fuels consist of moisture ranging from 5 to 35%. At the temperature above 100°C, the water is removed and converted into steam. Biomass sample does not experience any kind of decomposition in this zone.

2.3.2 Pyrolysis zone

Pyrolysis is the thermal decomposition of biomass in the absence of oxygen. The main reaction in this zone is the irreversible devolatilization reaction. Energy required for the reaction is obtained from the oxidation zone and temperature lies in between 200°C and 500°C.

Pyrolysis of biomass samples generally produces three types of products:

- Gases like H_2, CO, CH_4, H_2O, and CO_2
- Tar, a black, viscous and corrosive liquid
- Char, a solid residue containing carbon

2.3.3 Oxidation zone

This zone provides the energy for the gasification process i.e. for drying, pyrolysis and reduction. All these reactions are exothermic in nature (Kumar, et al., 2009 and Lendona, et. al., 2004). The combustion takes place within the at temperature range of 800°C to 1200°C. Heterogeneous reaction takes place between oxygen in the air and solid carbonized fuel producing carbon dioxide as per the following reaction.

$$C + O_2 \rightarrow CO_2 \quad (2.1)$$

Hydrogen in fuel reacts with oxygen in the air and blasts producing steam. It is expressed as follows.

$$H_2 + ½\ O_2 \rightarrow H_2O \quad (2.2)$$

2.3.4 Reduction zone

In the reduction zone, a number of high temperature chemical reactions take place in the absence of oxygen. The major reactions in this zone are water gas reaction, the water shift reaction, the boudouard reaction and methanation reaction. The fuel in this zone is in the highly carbonized form and red hot with all the volatile matters driven off and the temperature in this zone is in between 600°C and 800°C. These reactions are mentioned below.

Water gas reaction

$$C + H_2O \rightarrow CO + H_2 \quad (2.3)$$

Water shift reaction

$$CO + H_2O \rightarrow CO_2 + H_2 \quad (2.4)$$

Boudouard reaction

$$C + CO_2 \rightarrow 2CO \quad (2.5)$$

Methanation reaction

$$C + 2H_2 \rightarrow CH_4 \quad (2.6)$$

2.4 Types of Gasifiers

There are many types of gasifiers available ranging from simple to more complicated geometries. As there is an interaction of air or oxygen and biomass in the gasifier, they are classified according to the way air or oxygen is introduced into it. Thus there are 3 types of gasifiers.

- Fixed bed gasfiier (Up - draft, Down - draft)
- Fluidized bed gasifier (bubbling bed, circulating fluidized bed)
- Entrained bed gasifier

2.4.1 Fixed Bed Gasifier

2.4.1.1 Up-draft or Counter-current gasifier

It is the oldest and simplest type of gasifier. The up-draft gasifier consists of a fixed bed with carbonaceous fuel (e.g. coal or biomass) through which the gasifying agent (steam, oxygen, or air) flows in counter-current direction. Gasifying agent passes through the bed of biomass sample from bottom and the combustible gases come out from the top of the gasifier.

2.4.1.2 Down-draft or Co-current gasifier

The down-draft gasifier is similar to the counter-current type, but the gasifying agent flows in co-current configuration with the fuel i.e. downwards for which the name "down draft gasifier". Heat needs to be added to the upper part of the bed, either by combusting small amounts of the fuel or from external heat sources. This structure elevates the exiting temperature of the producer gas, helping tar cracking for which tar levels are much lower than in counter-current. The producer gas is removed at the bottom of the apparatus. Thus fuel and gas move in the same direction.

2.4.2 Fluidized Bed Gasifier

In a fluidized-bed gasifier, air or oxygen is injected upward at the bottom of solid fuel bed, suspending the fuel particles. Fluidized bed gasifiers are most useful for fuels that form highly corrosive ash that would damage the walls of slagging gasifiers. Biomass fuels generally contain high levels of corrosive ash. Fluidized bed allows an intensive mixing and a good heat transfers. Drying, pyrolysis, oxidation and reduction reactions take place simultaneously in the bed as it has no separated reduction zone. The temperature distribution in the fluidized bed is relatively constant and typically ranges from 700°C and 900°C.

Fluidized bed gasifiers are very easy to operate, easy to maintain, quick to start up, high combustion efficiency, give high output, rapid response to fuel input changes, uniform temperature in the bed, low restart time. Such gasifiers are simple in construction and reliable in operation. Therefore the present work is focused on optimization of fluidized bed gasifier.

2.4.3 Entrained Flow Gasifier

In entrained flow gasifier, a dry pulverized solid, an atomized liquid fuel or fuel slurry is gasified with oxygen in co-current flow configuration. The gasification reactions take place in a dense cloud of very fine particles. During the gasification such unit achieves high temperatures for which tar and methane are not present in the producer gas. The major part of the ash is removed as a slag because of the high operating temperature which is above the ash fusion temperature. However, an entrained-flow gasifier does have disadvantages that requires the highest amount of oxygen and produces the lowest heating value product gas. Entrained flow gasifiers are mainly preferred for gasification of hard coals.

2.5 Fluidized Bed Gasification

In a fluidized bed gasfiier the granular inert solids (usually silica sand) along with the feedstock are fluidized by the gasifying agent. Air is blown through a bed of solid particles at a sufficient velocity to keep these in a state of suspension. Gasification is an endothermic process for which the bed is originally heated externally and the feedstock is introduced as soon as a sufficiently high temperature is reached. The fuel particles are introduced at the bottom of the reactor, very quickly mixed with the bed material and almost instantaneously heated up to the bed temperature. As a result of this treatment, the fuel is pyrolysed very fast, resulting in a component mix with a relatively large amount of gaseous materials. Further gasification and tar-conversion reactions occur in the gas phase. Most systems are equipped with an internal cyclone in order to minimize char blow-out as much as possible. Ash particles are also carried over the top of the reactor and have to be removed from the gas stream if the gas is used in engine applications.

2.6 Advantages of Fluidized Bed Gasification

The fluidized bed gasification process has several advantages compared to simple burning process and other forms of gasification. Some of these advantages are described below:

- It is highly efficient as the overall thermal efficiency of fluidized bed gasifiers is typically in the range of 75% to over 90%, depending on the ash and moisture content of the fuel.
- In this gasifier air to fuel ratio can be changed which also helps to control the bed temperature in addition to the yield.
- Fluidized bed gasifiers are more tolerant to variation in feedstock as compared to other types of gasifiers.
- Such gasifiers maintain uniform radial temperature profiles and avoid slugging problems.
- Higher throughput of fuel as compared to other gasifiers.

Fluidized bed gasifier has capacity of Flexible Operations, because the process produces a fuel gas rather than just quantities of heat, which can be easily applied to a variety of industrial processes including boilers, dry kilns, veneer dryers or several pieces of equipment at once.

2.7 Disadvantages of Fluidized Bed Gasification

- Oxidizing conditions are created when oxygen diffuses from bubble to the emulsion phase there by reducing the gasification efficiency.
- Reduced solid conversion due to intimate mixing of fully and partially gasified fuels.
- Losses occurring due to particle entrainment.

2.8 Mechanism of Fluidized Bed Gasifier

Fluidization is one of the best ways of interacting solid particles with fluids when drag force acting on the solid particle and is equal to gravity force / weight of the particles. The fluidized bed is one of the best known contacting methods used in processing industries. The solid particles are transformed to fluid – like state through the contact with fluid i.e. gas or liquid or both which is allowed to pass through a distributor plate. Under the fluidized state, the gravitational force pull on solid particles is offset by the fluid drag force on them, thus the particles remain in a semi – suspended condition. At the critical value of fluid velocity, the upward drag force exerted by solid particles become exactly equal to the downward gravitational force, causing the solid particles to be suspended within the fluid. At this critical value, the bed is said to be just fluidized. Thereof the solid particles exhibit behaviors of fluid. This critical velocity is known as minimum fluidization velocity (Kunii et al, 1991). The different flow regimes of gas- solid fluidized bed resulted depending on the flow behavior is shown in Fig. 2.1.

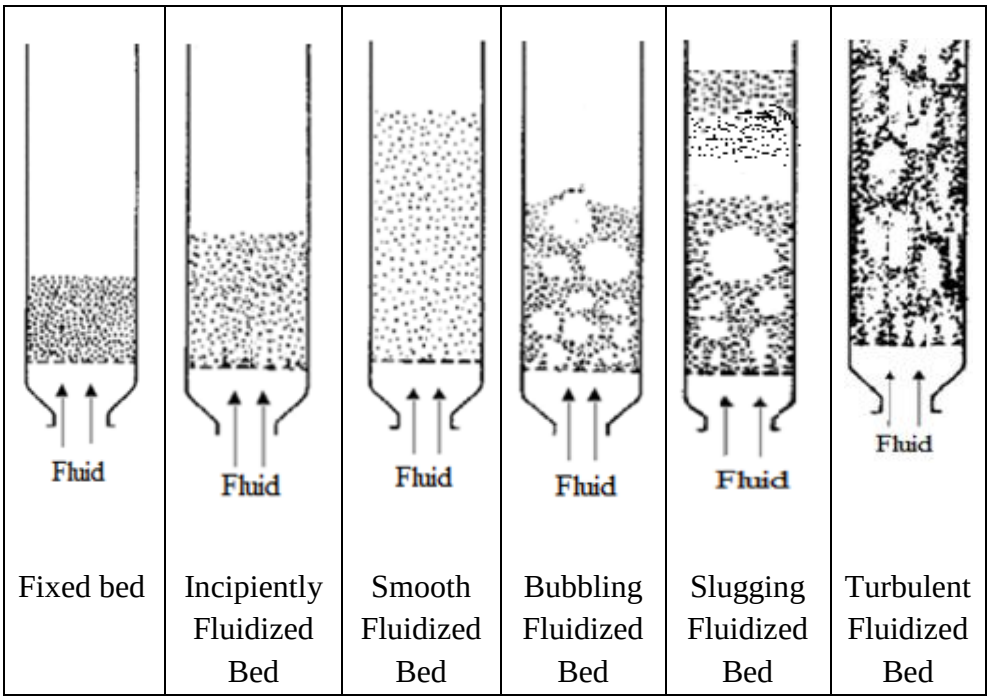

Fixed bed	Incipiently Fluidized Bed	Smooth Fluidized Bed	Bubbling Fluidized Bed	Slugging Fluidized Bed	Turbulent Fluidized Bed

Fig. 2.1 - Flow Regimes of Fluidized Bed (Kunii et al, 1991)

2.9 Computational Fluid Dynamics

Fluid (gas and liquid) flows are governed by partial differential equations (PDE) which represent conservation laws for the mass, momentum and energy. Computational Fluid Dynamics (CFD) is used to replace such PDE systems by a set of algebraic equations which can be solved using digital computers. The basic principle behind CFD modeling method is that the simulated flow region is divided into small cells. Differential equations of mass, momentum and energy balance are discretized and represented in terms of the variables at any predetermined position within the or at the center of cell. These equations are solved iteratively until the solution reaches the desired accuracy (ANSYS Fluent 13.0). CFD provides a qualitative prediction of fluid flows by means of

- Mathematical modeling (partial differential equations)
- Numerical methods (discretization and solution techniques)
- Software tools (solvers, pre- and post-processing utilities)

CFD simulation method is widely used to analyze the fluid flow behaviours as well as heat and mass transfer processes and chemical reactions. Due to a combination of increased computer efficacy and advanced numerical techniques, the numerical simulation techniques such

as CFD become a reality and offer an effective means of quantifying the physical and chemical process in the biomass thermo- chemical reactors under various operating conditions within a virtual environment. The resulting accurate simulations can help to optimize the system design and operation and understand the dynamic process inside the reactors. CFD modelling techniques are becoming widespread in the biomass thermo chemical conversion areas specifically in biomass gasification and combustion.

2.9.1 ANSYS FLUENT Software

FLUENT is one of the widely used CFD package. ANSYS FLUENT software contain wide range of physical modeling capabilities which are used to model flow, turbulence, reaction and heat transfer for industrial application. Features of ANSYS FLUENT software:

- MESH FLEXIBILITY: ANSYS FLUENT software provide mesh flexibility. It has ability to solve flow problem using unstructured mesh. Mesh type which support in FLUENT include quadrilateral, triangular, hexahedral, tetrahedral, polyhedral, pyramid and prism. Due to automatic nature of creating mesh saves time.
- MULTIPHASE FLOW: It is possible to model different fluids in a single domain in FLUENT.
- REACTION FLOW: Modeling of surface chemistry, combustion as well as finite rate chemistry can be done in FLUENT.
- TURBULENCE: It offers a number of turbulence models to study the effect of turbulence in a wide range of flow regimes.
- DYNAMICS AND MOVING MESH: The users setup the initial mesh and instruct the motion, while FLUENT software automatically changes the mesh to follow the motion instructed.
- POST-PROCESSING AND DATA EXPORT: Users can post process their data in FLUENT software, creating among other things contours, path lines and vectors to display the data.

2.10 Previous Works

Some of the various investigations done by researchers on gas-solid fluidization and gaification process in FB using CFD are mentioned below:

The flow and reaction in an entrained flow biomass gasifier has been simulated based on the CFX package where the phenomena of turbulent fluid flow, heat transfer, species transport, devolatilization, particle combustion, and gas phase chemical reactions are described (Fletcher et al. ,2000). Biomass particulate is modelled via a Lagrangian approach. The volatiles are released first as soon as the biomass is fed to the gasifier. Detailed information on the gas composition and temperature at the outlet are obtained from this model. Different operating scenarios are also allowed to be examined in an efficient manner.

The inert sand bed is modelled as a static isotropic porous media containing prescribed spherical volumes to model the presence of rising bubbles in a bubbling fluidized bed (Dimitrios, 2001). The biomass particles are modelled as Lagrangian particles. The drying and devolatilization of biomass, heterogeneous reactions of char and a single reaction in the gas phase converting water and methane into carbon monoxide and hydrogen are taken into account by this model. The simulated exhaust gas concentrations for a 3D gasifier are found to be agree reasonably well with measured data for H_2, O_2, CO_2, and H_2O but under predict CO_2 and over predict CO concentrations.

Hydrodynamics of a two-dimensional gas–solid fluidized bed reactor was studied experimentally and computationally (Taghipour et al., 2005). A multi fluid Eulerian model incorporating the kinetic theory for solid particles was applied to simulate the gas–solid flow. Momentum exchange coefficients were calculated using the Syamlal–O'Brien, Gidaspow, and Wen–Yu drag functions. The solid-phase kinetic energy fluctuation was characterized by varying the restitution coefficient values from 0.9 to 0.99.

A CFD model for fluidized bed biomass gasifier is developed and the simulations were carried out to obtain the optimal condition for production of hydrogen rich gas (Zhou et al., 2006). A non-premixed combustion model was used for biomass air-steam gasification in the gasifier. The simulation results were compared with the experimental data. The effects of the steam to biomass ratio(S/B), the equivalence ratio(ER), and the size of the biomass particles on the hydrogen yield were studied. The distributions of the hydrogen inside the gasifier at different conditions were also described.

Coal gasification in a bubbling fluidized bed gasifier was simulated using kinetic theory of granular flow (Liang, 2007**)**. The model considers instantaneous drying and devolatilization in the feed zone with proportion of products distribution resulting from experiments. Char is modelled as a single solid phase with constant particle size and heterogeneous reactions are included. Different cases for coal feed rate, air supply, steam supply and bed temperatures are investigated which gives good agreement between experimental and simulation results.

A 2D axisymmetric CFD model for the oxidation zone in a two-stage downdraft gasifier developed and simulated data fit satisfactorily to the experimental data regarding temperature pattern and tar concentration (Gerun et al., 2008). The simulations has shown the temperature profile in the reactor and predicted that the heat of reaction was released mainly close to the injector. The stream function and also the gas path lines were shown in the reactor. They found that gas path strongly depended on the initial departure point.

The fast pyrolysis of biomass in bubbling fluidized bed reactor was studied where the biomass particle was injected into the fluidized bed and the heat, momentum and mass transport from the fluidizing gas and fluidized sand is modeled (Papadikis and gu, 2008). The Eulerian approach was used to model the bubbling behaviour of the sand, which was treated as a continuum. Heat transfers from the bubbling bed to the discrete biomass particle, as well as biomass reaction kinetics were modelled according to the literature. The model predicted the radial distribution of temperature and product yields and also residence time of vapors and biomass particle.

A three-dimensional cfd model of a fluidized bed for sewage sludge gasifier for syngas described the complex physical and chemical phenomena in the gasifier, including turbulent flow, heat and mass transfer, and chemical reactions (Yiqun and Lifeng, 2008). The simulation employed the standard $\kappa - \varepsilon$ turbulence model for the gas phase in an Eulerian framework, and the discrete phase model for the sludge particles in a Lagrangian framework, coupled with the non-premixed combustion model for chemical reactions. The simulations provided detailed information on the gas products' composition and temperature distribution inside the gasifier and at the outlet. Effects of temperature and equivalence ratio (ER) on the product syngas (H_2 + CO) quality were also studied.

An overview of different CFD studies on thermo chemical biomass conversion including gasification and combustion processes in, e.g., fixed beds, furnaces, fluidized beds and wood

stoves was studied (Wang and Yan, 2008). Most of the cited work use commercial CFD codes with Euler–Lagrange modeling approaches. He stated that CFD can be used as a powerful tool to predict biomass thermo chemical processes as well as to design thermo chemical reactors. CFD has played an active part in system design including analysis the distribution of products, flow, temperature, ash deposit and NOx emission. The CFD model results are satisfactory and have made good agreements with the experimental data in many cases.

A 2-D, Eulerian multi fluid approach for gas-solid system in a CFB was carried out for simulation where Kinetic theory of granular flow (KTGF) has been used for describing the particle phase and K- ε based turbulent model has been used for gas phase (Yanping et al, 2009). The model was used for the examination of the effects of the feeding configuration on the gas/solid two-phase flow. In the present work, the simulations are conducted to come up to steady state fluidization and to predict the behaviour of a gas-solid fluidized bed using computational fluid dynamic technique.

The hydrodynamic behaviors of high-flux circulating fluidized beds (HFCFBs) with Geldart group B particles using a Eulerian multiphase model with the kinetic theory of granular flow (KTGF) was studied (Baosheng Jin et al. , 2010). The sensitivities of key model parameters (i.e., particle particle restitution coefficient (e), particle-wall restitution coefficient (e_w), and specularity coefficient (j)) on the predicted gas velocity, solids velocity, and solids volume fraction were tested. It was found that e has remarkable dependence on the particle diameter. Large-sized particles experience a more sensitive effect of e on predictions. The particle-wall restitution coefficient e_w has somewhat of an effect on the simulated values of gas velocity, solids velocity, and solids volume fraction. The specularity coefficient j has a slight effect on the gas velocity and solids velocity distributions but a pronounced effect on the solids volume fraction distribution. An increase in specularity coefficient results in a reduction in the solids volume fraction near the wall.

A multi fluid Eulerian modeling corporating the kinetic theory for solid particles was applied to simulate the unsteady state behavior of two dimensional non-reactive gas–solid fluidized bed reactor applying Computational Fluid Dynamics (CFD) techniques and momentum exchange coefficients were calculated by using the Syamlal-O'Brien drag functions and finite volume method was applied to discretize the equations (Hamzehei et al., 2010). Simulation results also indicated that small bubbles were produced at the bottom of the bed. These bubbles

collided with each other as they moved upwards forming larger bubbles. The effects of particle size and superficial gas velocity on hydrodynamics were also studied.

An Eulerian multiphase approach for modelling the gasification of wood in fluidized bed was developed where wood pyrolysis, char gasification and homogeneous gas phase reactions were taken into account (Gerber et al., 2010). The dispersed solid phase within the reactor was modeled as three continuous phases, i.e., one phase representing wood and two char phases with different diameters. 2D simulation results for a lab-scale bubbling fluidized bed reactor were presented and compared with experimental data for product gas and tar concentrations and temperature. They investigated the influence of two different classes of parameters on product gas concentrations and temperature: (i) operating conditions such as initial bed height, wood feeding rate, and reactor throughput and (ii) model parameters like thermal boundary conditions, primary pyrolysis kinetics, and secondary pyrolysis model. Two different pyrolysis models were implemented and are compared against each other.

The details of high resolution simulations of coal injection in a gasifier applying Computational Fluid Dynamics (CFD) a technique developed (Tingwen et al., 2010). This study demonstrated an approach to effectively combine high and low-resolution simulations for design studies of industrial coal gasifier. Effects of grid resolution and numerical discretization scheme on the predicted behavior of coal injection and gasification kinetics were analyzed. The result shown that for considering the inherent unsteady characteristics of the gasification process, it is necessary to use a high-order discretization scheme with low artificial diffusion. They concluded that fine grid resolution was always desired because of its predicted rich details in flow field and chemical reactions, which definitely improve the accuracy of numerical predictions.

Hydrodynamic behavior in a circulating fluidized bed (CFB) riser was developed by using Computational Fluid Dynamics (CFD) model (Peng et al., 2012). A new approach to specify the inlet boundary conditions that considering the inlet air jet effect was proposed in this study to simulate gas solid two-phase flows in circulating fluidized bed (CFB) risers more accurately. A computational fluid dynamics (CFD) model based on Eulerian- Eulerian approach coupled with kinetic theory of granular flow was adopted to simulate the flow using the proposed inlet boundary conditions. Simulation results were compared with experimental data. Good agreement between the numerical results and experimental data was observed under different operating conditions, which indicates the effectiveness and accuracy of the CFD model with the

proposed inlet boundary conditions. The result has shown that Inlet boundary conditions play an important role in accurately simulating the hydrodynamics and flow structures in the CFB riser. He also found that Particle size has an important effect on the flow in the CFB riser. Both experimental and numerical results illustrated a clear core annulus structure in the CFB riser under all operating conditions.

Hydrodynamic behaviour of a novel, self-heating biomass fast pyrolysis reactor named internally interconnected fluidized beds (IIFB) was studied (Zhang et al., 2011). The hydrodynamic characteristics of the reactor, such as solid circulation rate, pressure distribution, and volume fraction of particles were performed using numerical simulation in this study. Fluent 6.3, CFD commercial software, is used to calculate the model. A three-dimensional, non-steady-state, Eulerian multi-fluid model was used. The gas phase is modeled with a k-ε turbulent model, and the particle phase is modeled with the kinetic theory of granular flow.

CHAPTER THREE

CFD FORMULATION AND THEORY

3.1 Introduction

CFD is a powerful tool for the prediction of the fluid dynamics in various types of systems, thus, enabling a proper design of such systems. It is a sophisticated way to analyze not only for fluid flow behaviour but also for the processes of heat and mass transfer. The availability of affordable high performance computing hardware and the introduction of user-friendly interfaces have led to the development of CFD packages available both for commercial and research purposes. . In the field of fluidization, in particular, the use of CFD has pushed the frontier of fundamental understanding of fluid–solid interactions and has enabled the correct theoretical prediction of various macroscopic phenomena encountered in fluidized beds. The various general-purpose CFD packages in use are PHONICS, CFX, FLUENT, FLOW3D and STAR-CD etc. Most of these packages are based on the finite volume method and are used to solve fluid flow and heat and mass transfer problems.

The finite volume method (FVM) is one of the most versatile discrimination technique used for solving the governing equation for fluid flow, heat and mass transfer problems. The most compelling features of the FVM are that the resulting solution satisfies the conservation of quantities such as mass, momentum, energy and species transfer. In the FVM, the solution domain is subdivided into continuous cells or control volumes where the variable of interest is located at the centroid of the control volume forming a grid. The next step is to integrate the differential form of the governing equations over each control volume. Interpolation profiles are then assumed in order to describe the variation of the concerned variables between cell centroids. There are several schemes that can be used for discretization of governing equations e.g. central differencing, upwind differencing, power law differencing and quadratic upwind differencing schemes. The resulting equations are called discretized equation. In this manner the discretized equation expresses the conservation principle for the variable inside the control volume. This variable forms a set of algebraic equations which are solved simultaneously using special algorithm.

3.2 Problem Statement

Computational Fluid Dynamics (CFD) simulation is an economical and effective tool to study biomass gasification in a FBG. This study will investigate the bed dynamics, thermal-flow and gasification process in a fluidized bed gasifier. Biomass gasification is a multiphase reactive

flow phenomenon. It is a multiphase problem between gases and biomass particles and is also a reactive flow which involves homogeneous reactions among gases and heterogeneous reactions between biomass particles and gases. Both gas phase (primary phase) and solid phases (secondary phases) are solved by using Eulerian method. Both homogeneous (gas-gas) reaction and heterogeneous (gas-solid) reactions are simulated in this study.

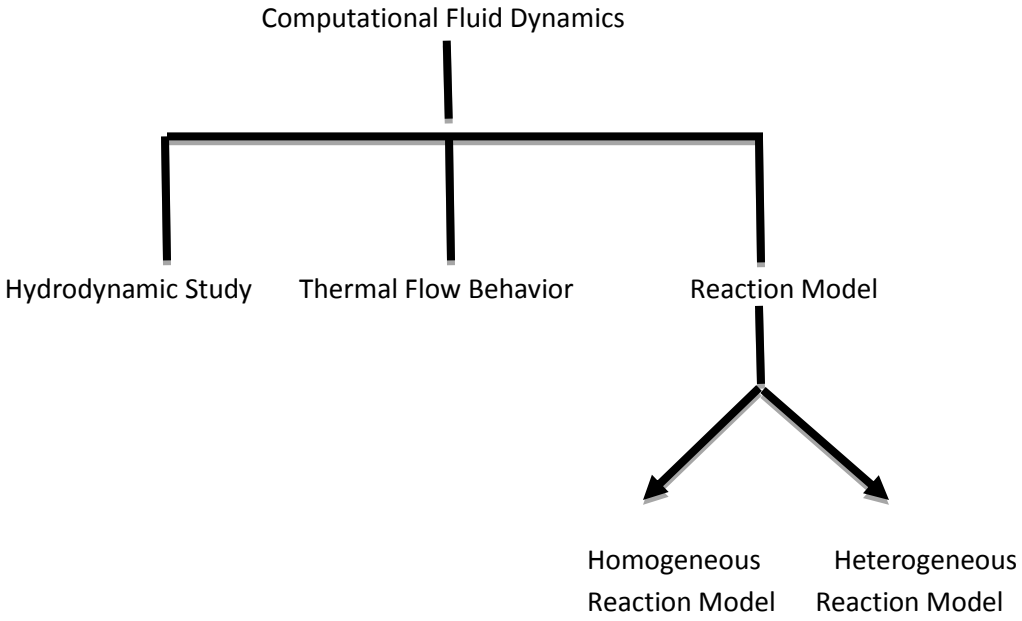

3.3 Computational Model

3.3.1 Physical Characteristics of the Problem

The physical characteristics of the problem are modeled as follows:

- The flow inside the domain is two dimensional, incompressible, and turbulent.
- Gravitational force is considered.
- Gas species involved in this study are Newtonian fluids with variable properties as functions of temperature. These variable properties are calculated by using piecewise polynomial method.
- Mass-weighted mixing-law for specific heat and incompressible-ideal gas for density is used for gas species mixture.
- The walls are impermeable and adiabatic.
- The flow is unsteady.
- No-slip condition (zero velocity) is imposed on wall surfaces.

3.3.2 General Governing Equations

The Eulerian- Eulerian method is adopted for this study. The governing equations for the conservations of mass, momentum, energy and species transfer are given below.

$$\frac{\partial \rho}{\partial t} + \nabla \cdot (\rho \vec{v}) = 0 \tag{3.1}$$

$$\frac{\partial}{\partial t}(\rho \vec{v}) + \nabla \cdot (\rho \vec{v}\vec{v}) = -\nabla p + \nabla \cdot (\bar{\bar{\tau}}) + \rho \vec{g} + \vec{F} \tag{3.2}$$

$$\frac{\partial}{\partial t}\left(\alpha_q \rho_q h_q\right) + \nabla \cdot \left(\alpha_q \rho_q \overrightarrow{u_q} h_q\right) = \alpha_q \frac{\partial P_q}{\partial t} + \bar{\bar{\tau}} : \nabla \overrightarrow{u_q} - \nabla \overrightarrow{q_q} + S_q + \sum_{p=1}^{n} \left(Q_{pq} + \dot{m}_{pq} h_{pq} - \dot{m}_{qp} h_{qp} \right) \tag{3.3}$$

$$\frac{\partial}{\partial t}(\rho Y_i) + \nabla \cdot (\rho \vec{v} Y_i) = -\nabla \cdot \vec{J}_i + R_i + S_i \tag{3.4}$$

3.3.3 Turbulence Model

The velocity field in turbulent flows always fluctuates. As a result, the transported quantities such as momentum, energy and species concentration fluctuate. The fluctuations can be small scale and high frequency which are computationally expensive to be directly simulated. To overcome this, a modified set of equations that are computationally less expensive to solve can be obtained by replacing the instantaneous governing equations with their time-averaged, ensemble-averaged, or otherwise manipulated to remove the small time scales. However, the modifications of the instantaneous governing equations introduce new unknown variables. Many turbulence models have been developed to determine these new unknown variables (such as Reynolds stresses or higher order terms) in terms of known variables or low order terms. This is so called "closure" of the turbulence models.

General turbulence models widely available are

- k-ε models (two equation)
  - Standard k-ε model
  - RNG k-ε model
  - Realizable k-ε model
- k-ω models (two equation)
  - Standard k-ω model
  - Shear-stress transport (SST) k-ω model

- Reynolds Stress model (five equation)

3.3.3.1 Standard k-ε Model

The standard k-ε model is employed in this study to simulate the turbulent flow due to its suitability for a wide range of wall-bounded and free-shear flows. The standard k-ε model is the simplest of turbulence two-equation model in which the solution of two separate transport equation allows the turbulent velocity and length scales, which are to be independently determined. The k-ε model is a semi-empirical model with several constants which were obtained from experiments.

All the three k-ε models have similar forms with major differences in the method of calculating the turbulent viscosity: the turbulent Prandtl numbers and the generation and destruction terms in the k-ε equations.

The standard k-ε model based on model transport equations for the turbulence kinetic energy (k) and its dissipation rate (ε). The turbulence kinetic energy, k, and its rate of dissipation, ε, are obtained from the following transport equations:

$$\frac{\partial}{\partial t}(\rho k) + \frac{\partial}{\partial x_i}(\rho k u_i) = \frac{\partial}{\partial x_j}\left[\left(\mu + \frac{\mu_t}{\sigma_k}\right)\frac{\partial k}{\partial x_j}\right] + G_k + G_b - \rho\varepsilon - Y_M + S_k \tag{3.5}$$

$$\frac{\partial}{\partial t}(\rho \varepsilon) + \frac{\partial}{\partial x_i}(\rho \varepsilon u_i) = \frac{\partial}{\partial x_j}\left[\left(\mu + \frac{\mu_t}{\sigma_\varepsilon}\right)\frac{\partial \varepsilon}{\partial x_j}\right] + C_{1\varepsilon}\frac{\varepsilon}{k}(G_k + C_{3\varepsilon}G_b) - C_{2\varepsilon}\rho\frac{\varepsilon^2}{k} + S_\varepsilon \tag{3.6}$$

In equations (3.3) and (3.4), G_k represents the generation of turbulence kinetic energy due to the mean velocity gradients and the Reynolds stress, calculated as:

$$G_k = \overline{-\rho u_\imath' u_\jmath'}\frac{\partial u_j}{\partial X_i} \tag{3.7}$$

G_b represents the generation of turbulence kinetic energy due to buoyancy, calculated as following:

$$G_b = \beta g_i \frac{\mu_t}{Pr_t}\frac{\partial T}{\partial X_i} \tag{3.8}$$

Pr_t is the turbulent Prandtl number and g_i is the component of the gravitational vector in the i^{th} direction. For standard k-ε model the value for Pr_t is set 0.85 in this study.

β is the coefficient of thermal expansion and is given as :

$$\beta = -\frac{1}{\rho}\left(\frac{\partial \rho}{\partial T}\right)_P \tag{3.9}$$

Y_M represents the contribution of the fluctuating dilatation in compressible turbulence to the overall dissipation rate, and is defined as:

$$Y_M = 2\rho\varepsilon M_t^{\,2} \tag{3.10}$$

Where M_t is the turbulent Mach number which is defined as:

$$M = \sqrt{\frac{k}{a^2}} \tag{3.11}$$

Where

$a\left(\equiv \sqrt{\gamma RT}\right)$= speed of sound

The turbulent (or eddy) viscosity,μ_t, is computed by combining k and ε as

$$\mu_t = \rho C_\mu \frac{k^2}{\varepsilon} \tag{3.12}$$

C1ε, C2ε, Cμ, σ_k and σ_ε are constants and their values are

C1ε = 1.44, C2ε = 1.92, Cμ = 0.09, σ_k = 1.0, and σ_ε = 1.3

3.3.4 Chemical Reaction Model

In this study, two different chemical reaction models are used in the CFD simulation: one for homogeneous gas-gas reactions and another for the heterogeneous (particle-gas) reactions. The key difference between these two models is related to how the carbon species are modeled. The homogeneous gas reaction assumes the carbon species gasified instantaneously, and the carbon is treated as a gas, while heterogeneous particle-gas reaction carbon as solid particles and they go through finite-rate reaction via a typical reaction at particle surface.

3.3.4.1 Instantaneous Gasification Model

The interphase exchange rates of mass, momentum and energy are assumed to be infinitely fast. Carbon particles are made to gasify instantaneously, thus the solid-gas reaction process can be modeled as homogeneous combustion reactions. This approach is based on the locally-homogeneous flow (LHF) model proposed by (Faeth, 1987), implying infinitely-fast interphase transport rates. The instantaneous gasification model can effectively reveal the overall combustion process and results without dealing with the details of the otherwise complicated heterogeneous particle surface reactions, heat transfer, species transport, and particle tracking in

turbulent reacting flow. The eddy-dissipation model is used to model the chemical reactions. The eddy-dissipation model assumes the chemical reactions are faster than the turbulence eddy transport, so the reaction rate is controlled by the flow motions.

The global instantaneous gasification mechanism is modeled to involve the following gaseous species: C, O_2, N_2, CO, CO_2, H_2O, H_2. All of the species are assumed to mix in the molecular level. In this approach, carbon is modeled as a gas species.

3.3.4.1.1 Eddy-dissipation Model

The assumption in this model is that the chemical reaction is faster than the time scale of the turbulence eddies. Thus, the reaction rate is determined by the turbulence mixing of the species. The reaction is assumed to occur instantaneously when the reactants meet. The net rate of production of species i due to reaction r, $R_{i,r}$, is given by the smaller of the two given expressions below:

$$R_{i.r} = v'_{I,r} M_{w,i} A \rho \frac{\varepsilon}{k} \min_R \left(\frac{Y_R}{v'_{R,r} M_{w,R}} \right) \quad (3.13)$$

$$R_{i.r} = v'_{i,r} M_{w,i} A B \rho \frac{\varepsilon}{k} \frac{\sum_P Y_P}{\sum_j^N v''_{j,r} M_{w,j}} \quad (3.14)$$

Where,

Y_P is the mass fraction of any product species, P

Y_R is the mass fraction of a particular reactant, R

A is an empirical constant equal to 4.0

B is an empirical constant equal to 0.5

$v'_{i,r}$ is the stoichiometric coefficient for reactant i in reaction r

$v''_{j,r}$ is the stoichiometric coefficient for product j in reaction r.

3.3.4.2 Finite-rate Reaction Model

The rate of chemical reaction is computed using an expression that takes into account temperature and pressure and ignores the effects of the turbulent eddies. In the finite-rate model, the reactions involve both homogeneous and heterogeneous reactions.

Homogeneous Reaction

Finite-Rate/Eddy-Dissipation model is used to simulate the homogeneous reactions. Reaction rate based on the Laminar Finite-Rate Model and Eddy-Dissipation Model are calculated and compared. The minimum of the two results is used as the homogeneous reaction

rate. The reason for taking the minimum reaction rate calculated from the eddy-dissipation model and finite rate model is, in practice, the Arrhenius rate acts as a kinetic "switch", preventing reaction before the flame holder; once the flame is ignited, the eddy-dissipation rate is generally smaller than the Arrhenius rate, and reactions are mixing-limited.

Laminar Finite-Rate Model

The laminar finite-rate model computes the chemical source terms using Arrhenius expressions, and ignores the effects of turbulent fluctuations. The net source of chemical species i due to reaction is computed as the sum of the Arrhenius reaction sources over the N_R reactions that the species participate in: and is given as

$$R_i = M_{w,i} \sum_{r=1}^{N_R} \hat{R}_{i,r} \tag{3.15}$$

Where $M_{w,i}$ is the molecular weight of species i and $\hat{R}_{i,r}$ is the Arrhenius molar rate of creation/destruction of species i in reaction r.

General form of r^{th} reaction:

$$\sum_{i=1}^{N_R} v'_{i,r} M_i \Leftrightarrow \sum_{i=1}^{N} v''_{i,r} M_i \tag{3.16}$$

Where

N = number of chemical species in the system

$v'_{i,r}$ = stoichiometric coefficient for reactant i in reaction r

$v''_{i,r}$ = stoichiometric coefficient for product i in reaction r

M_i = symbol denoting species i

For a non-reversible reaction, the molar rate of creation/destruction of species i in r^{th} reaction is given by:

$$\hat{R}_{i,r} = \Gamma\left(v''_{i,r} - v'_{i,r}\right)\left(k_{f,r} \prod_{j=1}^{N} [C_{j,r}]^{\left(\eta'_{j,r} + \eta''_{j,r}\right)}\right) \tag{3.17}$$

For a reversible reaction, the molar rate of creation/destruction of species i in reaction r is given by

$$\hat{R}_{i,r} = \Gamma\left(v''_{i,r} - v'_{i,r}\right)\left(k_{f,r} \prod_{j=1}^{N} [C_{j,r}]^{\eta'_{j,r}} - k_{b,r} \prod_{j=1}^{N} [C_{j,r}]^{\eta''_{j,r}}\right) \tag{3.18}$$

Where,

$C_{j,r}$ = molar concentration of each reactant and product species j in reaction r ($kgmol/m^3$)

$\eta'_{j,r}$ = forward rate exponent for each reactant and product species j in reaction r

$\eta''_{j,r}$ = backward rate exponent for each reactant and product species j in reaction r

$k_{f,r}$ = forward rate constant for reaction r

$k_{b,r}$= backward rate constant for reaction r

Γ represents the net effect of third bodies on the reaction rate and is given by

$$\Gamma = \sum_j^N \gamma_{j,r} C_j \tag{3.19}$$

Where $\gamma_{j,r}$ is the third body efficiency of the j^{th} species in the r^{th} reaction.

The forward rate constant for reaction r, $k_{f,r}$ is computed using the Arrhenius expression

$$k_{f,r} = A_r T^{\beta r} e^{-E_r/RT} \tag{3.20}$$

Where

A_r = pre-exponential factor (consistent unit)

βr = temperature exponent (dimensionless)

E_r = activation energy for the reaction (J/kgmol)

R = universal gas constant (J/kg mol-K).

If the reaction is reversible, the backward rate constant for reaction r, $k_{b,r}$ is computed from the forward rate constant using the following relation:

$$k_{b,r} = \frac{k_{f,r}}{k_r} \tag{3.21}$$

Where Kr is the equilibrium constant for the r^{th} reaction

Heterogeneous Reaction

The particle reaction, R (kg/m^2-s), is expressed as:

$$R = D_0(C_g - C_s) = R_c(C_s)^N \tag{3.22}$$

Where

D_0= bulk diffusion coefficient (m/s)

C_g= mean reacting gas species concentration in the bulk (kg/m3)

C_s= mean reacting gas species concentration at the particle surface (kg/m2)

R_c= chemical reaction rate coefficient

N = apparent reaction order (dimensionless)

The concentration at the particle surface, Cs, is not known, so it is eliminated and the expression is as follows.

$$R = R_c \left[C_g - \frac{R}{D_0} \right]^N \tag{3.23}$$

The reaction stoichiometry of a particle undergoing an exothermic reaction in a gas phase is given as

Particle species j (s) + gas phase species n $\rightarrow$ products.

Its reaction rate is given as:

$$\overline{R}_{j,r} = A_p \eta_r Y_j R_{j,r} \tag{3.24}$$

$$R_{j,r} = R_{kin,r} \left(P_n - \frac{R_{j,r}}{D_{0,r}} \right)^{N_r} \tag{3.25}$$

Where

$\overline{R}_{j,r}$ = rate of particle surface species depletion (kg/s)

A_p = particle surface area (m^2)

Y_j = mass fraction of surface species j in the particle

η_r = effectiveness factor (dimensionless)

$R_{j,r}$= rate of particle surface species reaction per unit area (kg/m^2-s)

P_n = bulk partial pressure of the gas phase species (Pa)

$D_{0,r}$ = diffusion rate coefficient for reaction r

$R_{kin,r}$ = kinetic rate of reaction r

N_r = apparent order of reaction r.

The kinetic rate of reaction r is defined as:

$$R_{kin,r} = A_p T^{\beta} e^{-\left(E_r / RT\right)} \tag{3.26}$$

3.4 Computational Scheme

3.4.1 Solution Methodology

There are three major steps for solving a CFD problem. These are

- Pre-processing
- Solver
- Post-processing

3.4.1.1 Preprocessing

This is the first step in solving any CFD problem. It basically involves designing and building the domain. It involves the following steps:

- Definition of the geometry of the region: The computational domain.
- Grid generation, the subdivision of the domain into a number of smaller, non-overlapping sub domains (or control volumes or elements Selection of physical or chemical phenomena that need to be modeled).
- Definition of fluid properties.
- Specification of appropriate boundary conditions at cells, which coincide with or touch the boundary.

The solution to a flow problem (velocity, pressure, temperature etc.) is defined at nodes inside each cell. The accuracy of a CFD solution is governed by the number of cells in the grid. In general, the larger numbers of cells better the solution accuracy. Geometry and mesh generating software GAMBIT is used to draw complex geometry. GAMBIT is a state-of-the-art preprocessor for engineering analysis. Quad meshes are used in the simplified 2-D domain. Once computational domain geometry has been meshed in GAMBIT, it is imported into the commercial CFD code ANSYS FLUENT 13.0 from ANSYS, Inc. Then, the appropriate models and boundary conditions are set.

3.4.1.2 Solver

After the geometry has been made then the next step is to do the flow calculations. Calculations are performed to obtain the solution for the governing equations. CFD solver does the flow calculations and displays the results obtained. FLUENT, FloWizard, FIDAP, CFX and POLYFLOW are some of the types of solvers. Numerous iterations are performed till the solution converges and the results obtained. The first step is the setting of the under relaxation factors which are essential for the solution convergence as wrong or improper under relaxation factors can hamper the convergence. Initialization of the solution is also as important as setting under relaxation factors because it helps the solver to assume some initial values required to solve the governing equations involved. ANSYS FLUENT is a finite-volume based CFD solver written in language "C" and has the ability to solve fluid flow, heat transfer and chemical reactions in complex geometries and supports both structured and unstructured mesh.

3.4.1.3 Post processing

This is the final step in CFD analysis, and it involves the organization and interpretation of the predicted flow data and the production of CFD images and animations. Charts and various visualization schemes can be employed to aid in understanding the physics of the solution. The results are presented in the form of x-y plots, contour plots (e.g. temperature contour), velocity vector plots, streamline plots, and animations via the built-in plotting software in ANSYS/Fluent.

3.4.2 Numerical Procedure

For performing the simulation in ANSYS FLUENT 13.0 the procedures are

- Create and mesh the geometry model using GAMBIT
- Import geometry into ANSYS FLUENT 13.0
- Define the solver model
- Define the turbulence model
- Define the species model
- Define the materials and the chemical reactions
- Define phases: primary and secondary phase
- Define phase Interaction such as drag force, heterogeneous reaction etc.
- Define the boundary conditions
- Define region adaptation and patching
- Initialize the calculations
- Iterate/calculate until convergence is achieved
- Post processes the results.

ANSYS FLUENT 13.0 has two solution methods: (a) Pressure based solution method and (b) Density based solution method. Pressure based solution method solves the governing equations of continuity, momentum, energy, and species transport equations sequentially. In the Pressure based solution, the non-linear governing equations are implicitly linearized, which means that each unknown value is computed using a relation that includes both existing and unknown values from neighbouring cells. As a result, each unknown will appear in more than one equation in the linear system produced. Thus, these equations must be solved simultaneously in order to obtain the unknown quantities. In this work pressure based solution method is taken.

The governing equations are discretized spatially to yield discrete algebraic equations for each control volume. There are several discretization schemes available in ANSYS FLUENT as follows.

- First Order
- Second Order
- Power Law and
- QUICK

In the present study the second order scheme is used as the discretization scheme for momentum, turbulence kinetic energy "k" and dissipation rate "ε", energy, species equations. Volume fraction of solid phase uses the First Order or QUICK scheme.

ANSYS FLUENT also provides three algorithms for pressure velocity coupling in the Pressure Based solver:

- SIMPLE
- SIMPLEC and
- PISO

The SIMPLE algorithm (Patankar et. al, 1980) is used in this study to couple the pressure and velocity. The built-in standard k-ε turbulence model is used, and the model constants C1ε, C2ε, Cμ, σ_k and σ_ε have the following values,

C1ε = 1.44, C2ε = 1.92, Cμ = 0.09, σ_k = 1.0, and σ_ε = 1.3.

The following boundary conditions on the surface geometry have been taken for the present work in GAMBIT.

- Velocity inlet: All the inlet surfaces are defined as velocity inlets. The velocity, temperature, and the mass fractions of all species of the gas mixture are specified.
- Pressure outlet: The outlet surface is assigned as a pressure outlet boundary. Pressure, temperature, and species mass fractions of the gas mixture just downstream of the outlet (outside the domain) are specified.
- Walls: The outside surfaces are defined as wall boundary. The walls are stationary with no-slip condition imposed (zero velocity) on the surface.

The detailed steps of the calculation process are given below.

1. Initially the physical properties and exchange coefficients are calculated.

2. The momentum equations are solved using the current values of pressure and face mass fluxes to get the updated velocity field.
3. Equation for the pressure correction is calculated from the continuity equation, and the linearized momentum equations since the velocity field obtained in step (2) may not satisfy the continuity equation.
4. The pressure correction equations obtained from step (3) are solved to correct the pressure and velocity fields, and face mass such that the continuity equation is satisfied.
5. The equations for turbulence are solved using the updated values of the other variables.
6. The homogeneous gas phase reactions are solved. Production and consumptions of each species are calculated.
7. Enthalpy changes due to reaction are calculated.
8. The species transport equations are solved. Changes in the species mass fraction due to reactions in steps (6) and (12) appear as source or sink terms in the species transport equation.
9. The energy equation is solved. This includes source or sink terms due to reactions in steps (6) and (7).
10. Forces on the particles (secondary phase) such as drag force, lift force, virtual mass force are calculated.
11. Particles (secondary phase) heat transfer are calculated.
12. Heterogeneous reactions (gas-solid) are calculated. Production and consumptions of each species are calculated.
13. Enthalpy changes due to reaction are calculated.
14. The species transport equations are solved. Changes in the species mass fraction due to reactions in steps (12) appear as source or sink terms in the species transport equation.
15. The energy equation is solved. This includes source or sink terms due to reactions in steps (13) and (14).
16. Primary phase properties are updated based on the secondary phase.
17. The equation is checked for convergence.
18. If convergence criteria are met, the process is stopped. Otherwise, the process is repeated from step (1).

CHAPTER FOUR

MODELING MULTIPHASE FLOWS

4.1 Introduction

A large number of flows encountered in nature and technology are a mixture of phases. Physically phases of matter are gas, liquid and solid. But the concept of phase in a multiphase flow can be defined as an identifiable class of material that has an inertial response to system, interaction with the flow and the potential field in which it is immersed

4.2 Multiphase Flow Regime

Multiphase flow regimes can be grouped into four categories:

- Gas-liquid or liquid-liquid flows
- Gas-solid flows
- Liquid-solid flows and
- Three-phase flow

4.2.1 Gas-liquid or Liquid-liquid Flows

The following regimes are known as gas-liquid or liquid-liquid flows:

- Bubbly flow: This is the flow of fluid bubbles or discrete gaseous in a continuous fluid. Such flows are found in many processes. Example: absorption process, aeration process, air lift pumps, cavitations, evaporation, flotation, and scrubbers.
- Gas-droplet flow: This is the flow of discrete fluid droplets in a continuous gas phase medium. Example: flow in atomizers, combustors, cryogenic pump, dryers, evaporater, gas cooler, and scrubbers.
- Slug flow: This is the flow of large bubbles in a continuous fluid medium. Example: large bubble motion in pipes or tanks.
- Stratified/free-surface flow: This is the flow of immiscible fluids separated by an interface. Example: sloshing in offshore separator devices and boiling and condensation in nuclear reactors.

4.2.2 Gas-solid Flows

The following regimes are known as gas-solid flows

- Gas-particle flows: This is the flow of discrete particles in a continuous gas phase. Example: flow in cyclone separators, air classifiers, dust collectors and dust-laden environmental flows.

- Flow by pneumatic transport: This is the flow that depends on solid loading, Reynolds numbers, and particle properties. Example: transport of cement, grains, and metal powders.
- Flow by fluidized bed: This consists of a vertical cylinder containing particles, into which a gas is introduced through a distributor which raises the bed of particles. Depending on the gas flow rate, bubbles appear and rise through the bed intensifying the mixing within the bed. Example: fluidized bed reactors, fluidized bed boiler, fluidized bed gasifier and fluidized bed combustors.

4.2.3 Liquid-solid Flows

The following regimes are known as liquid-solid flows:

- Slurry flows: This flow is the transport of particles in liquids. Example: slurry transport and mineral processing.
- Hydro-transport: This is the flow that describes densely-distributed solid particles in a continuous liquid. Example: mineral processing and biomedical and physiochemical fluid systems.
- Sediment transport: This is the flow that describes a tall column initially containing a uniform dispersed mixture of particles. At the bottom, the particles will slow down and form a sludge layer. Example: mineral processing.

4.2.4 Three-phase Flows

Three-phase flows are combinations of the other flow regimes as listed above.

- Bubbles in a slurry flow
- Droplets/particles in gaseous flows

4.3 Approaches to Multiphase Modeling

Advance in computational fluid mechanics have provided the basis for further insight into the dynamics of multiphase flow. There are two approaches widely used for the numerical calculation of multiphase flows as mentioned below.

- Euler-Lagrange approach
- Euler-Euler approach

4.3.1 The EULER-LAGRANGE Approach

The Lagrangian discrete phase model follows the Euler-Lagrange approach. The fluid phase is treated as a continuum by solving the time-averaged Navier-Stokes equations, while the dispersed phase is solved by tracking a large number of particles, bubbles, or droplets through the calculated flow field. The dispersed phase can exchange momentum, mass and energy with the fluid phase. A fundamental assumption made in this model is that the dispersed second phase occupies a low volume fraction, even though high mass loading, (mass of particle >= mass of fluid) is acceptable. The particle or droplet trajectories are computed individually at specified intervals during the fluid phase calculation. This makes the model appropriate for the modeling of spray dryers, coal and liquid fuel combustion, and some particle laden flows, but inappropriate for the modeling of liquid-liquid mixtures, fluidized beds or any application where the volume fraction of the second phase is not negligible (Mahapatra and Rakh, 2007).

4.3.2 The EULER-EULER Approach

In the Euler-Euler approach the different phases are treated mathematically as interpenetrating continua. Since the volume of a phase cannot be carried occupied by the other phases, the concept of the volume fraction is introduced. These volume fractions are assumed to be continuous functions of space and time and their sum is equal to one. Conservation equations for each phase are derived to obtain a set of equations, which have similar structure for all phases. These equations are closed by providing constitutive relations that are obtained from empirical information or in the case of granular flows by application of kinetic theory (Kumar, 2009).

There are three different Euler-Euler multiphase models available:

- The volume of fluid (VOF) model
- The Mixture model
- The Eulerian model

4.3.2.1 The VOF Model

The VOF model is a surface-tracking technique applied to a fixed Eulerian mesh. It is designed for two or more immiscible fluids where the position of the interface between the fluids is of interest. In the VOF model, a single set of momentum equations is shared by the fluids and the volume fraction of each of the fluids in each computational cell is tracked throughout the domain. The applications of VOF model include stratified flows, free surface flows, filling,

sloshing, and the motion of large bubbles in a liquid, the motion of liquid after a dam break, the prediction of jet breakup (surface tension) and the steady or transient tracking of any liquid- gas interface.

4.3.2.2 The Mixture Model

The mixture model is designed for two or more phases (fluid or particulate). As in the Eulerian model, the phases are treated as interpenetrating continua. The mixture model solves for the mixture momentum equation and prescribes relative velocities to describe the dispersed phase.

Applications of the mixture model include particle-laden flows with low loading, bubbly flows, and sedimentation and cyclone separators. The mixture model can also be used to model homogeneous multiphase flow with strong coupling without relative velocities for the dispersed phases. In addition, the mixture model can be used to calculate non-Newtonian viscosity. This model is suitable for flows in which the dispersed-phase volume fractions are less than or equal to 10%.

4.3.2.3 The Eulerian Model

The Eulerian model is the most complex of the multiphase model in ANSYS FLUENT. It solves a set of *n* momentum and continuity equations for each phase. Through the pressure and interphase exchange coefficients, coupling are achieved. The manner in which this coupling is handled depends upon the type of phases involved. Granular (fluid solid) flows are handled differently than non-regular (fluid-fluid) flows. For granular flows, the properties are obtained from the application of kinetic theory. Momentum exchange between the phases is also dependent upon the type of mixture being modeled.

Choosing Appropriate Model:

An appropriate multiphase model for the multiphase system can be determined from the flow regime. For slug, and stratified/free surface flows VOF model are used. For slurry flow, hydro transport, bubbly, droplet, and particle-laden flows in which the phase mix and/or dispersed phase volume fractions exceed 10% either mixture model or Eulerian model are used. For general, complex multiphase flows that involve multiple flow regimes, select the aspect of flow that is of most interest and choosing of model that is of most appropriate.

To choose between the mixture and Eulerian model some guideline are considered:

- If there is a wide distribution of the dispersed phase, the mixture model may be preferable. If the dispersed phase are concentrated just in a portion of domain the Eulerian model is used instead.
- If the interphase drag laws are applicable to the system, the Eulerian model can usually provide more accurate results than the mixture model. Even though same drag laws can be applied to the mixture model, also for non-granular Eulerian simulation , if the interphase drag laws are unknown on their applicability to the system is questionable the mixture model maybe a better choice.
- To solve a simple problem which requires less computational effort, the mixture model may be a better option since it solves a smaller number of equations then the Eulerian model. If accuracy is more important than computational effort, the Eulerian model is a better choice.

4.4 EULERIAN Multiphase Model Theory

In the present work, an Eulerian granular multiphase model is adopted where gas and solid phases are all treated as continua, interpenetrating and interacting with each other everywhere in the computational domain. With the Eulerian multiphase model, the number of secondary phase is limited only by memory requirement and convergence behaviour. Any number of secondary phases can be modeled provided that sufficient memory is available. Eulerian multiphase model does not distinguish between fluid-fluid and fluid-solid (granular) multiphase flows. A granular phase is simple one that involves at least one phase that has been designated as a granular phase. The pressure field is assumed to be shared by all the three phases, in proportion to their volume fractions. Solid-phase shear and bulk viscosities are obtained by applying kinetic theory of granular flows.

4.4.1 Governing Equations

4.4.1.1 Volume Fraction Equation

Volume fractions represent the space occupied by each phase, and the laws of conservation of mass and momentum are satisfied by each phase individually. The derivation of the conservation equations can be obtained by ensemble averaging the local instantaneous balance for each of the phases or by using the mixture theory approach.

The Volume of Phase q, V_q is defined by

$$V_q = \int_0^v \alpha_q \, . \, dV \tag{4.1}$$

Where

$$\sum_{q=1}^{n} \alpha_q = 1 \tag{4.2}$$

The effective density of phase q is calculated as

$$\vec{\rho}_q = \alpha_q . \rho_q \tag{4.3}$$

Where ρ_q is the physical density of the phase q**.**

4.4.1.2 Conservation Equations

The motion of each phase is governed by respective mass, momentum and energy conservation equations.

Conservation of mass:

The Continuity equation for phase q is

$$\frac{\partial}{\partial t}\left(\alpha_q \rho_q\right) + \nabla . \left(\alpha_q \rho_q \vec{v}_q\right) = \sum_{p=1}^{n}\left(\dot{m}_{pq} - \dot{m}_{qp}\right) + S_q \tag{4.4}$$

Where

$\vec{v}_q$ = Velocity of phase q

$\dot{m}_{pq}$ = the mass transfer from phase q to phase p

$\dot{m}_{qp}$ = the mass transfer from phase p to phase q

S_q = the source term of phase q

The right-hand side of Equation (4.4) is zero. This is because the net mass transfer from one phase to another is zero and the source term is considered by default zero except for the constant user-defined boundary conditions. Thus we have the following continuity equations:

Gas phase:

$$\frac{\partial}{\partial t}\left(\alpha_g \rho_g\right) + \nabla . \left(\alpha_g \rho_g \vec{v}_g\right) = 0 \tag{4.5}$$

Solid phase:

$$\frac{\partial}{\partial t}\left(\alpha_s \rho_s\right) + \nabla . \left(\alpha_s \rho_s \vec{v}_s\right) = 0 \tag{4.6}$$

Conservation of momentum:

Newton's second law of motion states that the change in momentum equals the sum of forces on the domain.

The momentum equation for phase q yields

$$\frac{\partial}{\partial t}(\alpha_q \rho_q \vec{v}_q) + \nabla.(\alpha_q \rho_q \vec{v}_q \vec{v}_q) = -\alpha_q \nabla. p + \nabla. \bar{\bar{\tau}}_q + \alpha_q \rho_q \vec{g} + \sum_{p=1}^{n} (\vec{R}_{pq} + \dot{m}_{pq} \vec{v}_{pq} - \dot{m}_{qp} \vec{v}_{qp}) + (\vec{F}_q + \vec{F}_{lift,q} + \vec{F}_{vm,q}) \quad (4.7)$$

Where $\bar{\bar{\tau}}_q$ is the q^{th} phase stress-strain tensor

$$\bar{\bar{\tau}}_q = \alpha_q \mu_q (\nabla. \vec{v}_q + \nabla. \vec{v}_q^T) + \alpha_q \left(\lambda_q - \frac{2}{3}\mu_q\right) \nabla. \vec{v}_q \bar{\bar{I}} \quad (4.8)$$

Where

μ_q = the shear viscosity of phase q

λ_q = the bulk viscosity of phase q

$\vec{F}_q$ = an external body force of phase q

$\vec{F}_{lift,q}$ = a lift force of phase q

$\vec{F}_{vm,q}$ = a virtual mass force of phase q

$\vec{R}_{pq}$ = an interaction force between phase p and q

p = pressure shared by all phases

$\vec{v}_{pq}$ is the interphase velocity and is defined as follows. If $\dot{m}_{pq} > 0$(i.e., phase p mass is being transferred to phase q), $\vec{v}_{pq} = \vec{v}_p$; If $\dot{m}_{pq} < 0$ (i.e., phase q mass is being transferred to phase p), $\vec{v}_{pq} = \vec{v}_q$. Similarly if $\dot{m}_{qp} > 0$, then $\vec{v}_{qp} = \vec{v}_q$; if $\dot{m}_{qp} < 0$, then $\vec{v}_{qp} = \vec{v}_p$.

The $\vec{F}_{vm,q}$, virtual mass force and the lift force $\vec{F}_{lift,q}$ are considered zero by default. The equation 4.7 must be closed with appropriate expressions for the interphase force. The program uses a simple interaction term, in the following form:

$$\sum_{p=1}^{n} \vec{R}_{pq} = \sum_{p=1}^{n} Kpq\left(\vec{v}_p - \vec{v}_q\right)$$

Where Kpq (= Kqp) is the interphase momentum exchange coefficient.

Thus considering the above and $\dot{m}_{pq} = \dot{m}_{qp} = 0$, the general equations take the following form for the gas and solid phases.

Gas phase:

$$\frac{\partial}{\partial t}\left(\alpha_g \rho_g \vec{v}_g\right) + \nabla.\left(\alpha_g \rho_g \vec{v}_g \vec{v}_g\right) = -\alpha_g \nabla.p + \nabla.\bar{\bar{\tau}}_g + \alpha_g \rho_g \vec{g} + Ksl\,(\vec{v}_g - \vec{v}_s) \quad (4.9)$$

Solid phase:

$$\frac{\partial}{\partial t}(\alpha_s \rho_s \vec{v}_s) + \nabla.(\alpha_s \rho_s \vec{v}_s \vec{v}_s) = -\alpha_s \nabla.p + \nabla.\bar{\bar{\tau}}_s + \alpha_s \rho_s \vec{g} + Ksl\,(\vec{v}_g - \vec{v}_s) \quad (4.10)$$

Conservation of Energy:

To describe the conservation of energy in Eulerian multiphase applications, a separate enthalpy equation is written for each phase:

$$\frac{\partial}{\partial t}\left(\alpha_q \rho_q h_q\right) + \nabla \cdot \left(\alpha_q \rho_q \overrightarrow{u_q} h_q\right) = \alpha_q \frac{\partial P_q}{\partial t} + \bar{\bar{\tau}} : \nabla \overrightarrow{u_q} - \nabla \overrightarrow{q_q} + S_q + \sum_{p=1}^{n} (Q_{pq} + \dot{m}_{pq} h_{pq} - \dot{m}_{qp} h_{qp}) \quad (4.11)$$

Where

h_q = the specific enthalpy of the phase "q"

$\overrightarrow{q_q}$ = the heat flux of the phase "q"

Sq = a source term that includes sources of enthalpy

Q_{pq} = the intensity of heat exchange between the phase "p" and "q"

h_{pq}= the inter-phase enthalpy

4.4.1.3 Interphase Exchange Coefficient

4.4.1.3.1 Fluid-solid Exchange Coefficient

The fluid-solid exchange coefficient K_{sl} can be written in the following general form:

$$K_{sl} = \frac{\alpha_s \rho_s f}{\tau_s} \quad (4.12)$$

Where f is defined differently for the different exchange coefficient model and τ_s**,** the particulate relaxation time is expressed as follows:

$$\tau_s = \frac{\rho_s d_s^2}{18\,\mu_l} \tag{4.13}$$

where d_s is the diameter of the particles of phase *s.* All definition of f includes a drag function *(*C_D*)* that is based on the relative Reynolds number *(*Re_s*).* It is this drag function that differs among the exchange co-efficient models.

In the present study, Gidaspow model has been used, which is the combination of Wen and Yu model and the Ergun equation When$\alpha_l > 0.8$**,** the fluid solid exchange coefficient K_{sl} is of the following form:

$$K_{sl} = \frac{3}{4} C_D \frac{\alpha_s \alpha_l \rho_l |\vec{v}_s - \vec{v}_l|}{d_s} \alpha_l^{-2.65} \tag{4.14}$$

Where

$$C_D = \frac{24}{\alpha_l Re_s}[\,1 + 0.15(\alpha_l Re_s)^{0.687}] \tag{4.15}$$

Where Re_s is defined as

$$Re_s = \frac{\rho_l d_s |\vec{v}_s - \vec{v}_l|}{\mu_l} \tag{4.16}$$

l is the l^{th} fluid phase, *s* is for the s^{th} solid phase particles and d_s is the diameter of the s^{th} solid phase particles

When $\alpha_l \leq 0.8$, K_{ls} is written as

$$K_{ls} = \frac{3(1+e_{ls})\left(\frac{\pi}{2} + C_{fr,ls}\frac{\pi^2}{8}\right).\alpha_s \rho_s \alpha_l \rho_l (d_l + d_s)^2 g_{0,ls} |\vec{v}_l - \vec{v}_s|}{2\pi(\rho_l d_l^3 + \rho_s d_s^3)} \tag{4.17}$$

Where

e_{ls} = the specific enthalpy of the phase "q"

$C_{fr,ls}$ = the coefficient of friction between the l^{th} and s^{th} solid phase particles.

d_l = diameter of the particle of solid l

$g_{0,ls}$ = the radial distribution coefficient

4.4.1.3.2 Solid-solid Exchange Coefficient

The symmetric Syamlal (1987) model is recommended for a pair of solids where the solid-solid exchange coefficient K_{ls} has the following form:

$$K_{ls} = \frac{3(1+e_{ls})+\left(\frac{\pi}{2}+C_{fr,ls}\frac{\pi^2}{8}\right)\alpha_s\rho_s\alpha_l\rho_l(d_l+d_s)^2 g_{0}l_s}{2\pi(\rho_l d^3{}_l+\rho_s d^3{}_s)}|\vec{v}_s - \vec{v}_l| \quad (4.18)$$

Where

e_{ls} = the restitution coefficient

$C_{fr,ls}$= the coefficient of friction between the l^{th} and s^{th} solid-phase particles ($C_{fr,ls}$= 0)

d_l= the diameter of the particles of solid l

$g_0 l_s$= the radial distribution coefficient

4.4.1.4 Solid Pressure

For granular flow in the compressible regime (i.e. where the solid volume fraction is less than its maximum allow value), a solid pressure is calculated independently and used for the pressure gradient term ($\nabla . p_s$) in the granular-phase momentum equation. Because a Maxwellian velocity distribution is used for the particles, a granular temperature is introduced into the model which appears in the expression for the solid pressure and viscosities. The solid pressure is composed of a kinetic term and a secondary term due to particle collisions.

$$p_s = \alpha_s\rho_s\Theta_s + 2\rho_s(1+e_{ss})\alpha_s^2 g_{0,ss}\Theta_s \quad (4.19)$$

Where

e_{ss} = the co-efficient of restitution for particle collisions

$g_{0,ss}$= the radial distribution function

Θ_s = the granular temperature

The granular temperature Θ_s is proportional to the kinetic energy of the fluctuating particle motion. In ANSYS FLUENT a default value of 0.9 for Θ_s is used and can be adjusted to suit the particle type. The function $g_{0,ss}$ is a distribution function that governs the transition from the "compressible" condition with $\alpha_s < \alpha_{s,max}$ (where the spacing between the solid particles can continue to decrease) to incompressible condition with $\alpha = \alpha_{s,max}$ (where there is no further decrease in space). The default value for$\alpha_{s,max}$ is taken as0.63.

4.4.1.5 Radial Distribution Function

The radial distribution function g_o is a correction factor that modifies the probability of collision between grains when the solid granular phase becomes dense. This function may also be interpreted as the non-dimensional distance between spheres as mentioned below:

$$g_o = \frac{s + d_p}{s} \tag{4.20}$$

where s = the distance between grains and d_p = the diameter of particle.

From equation (4.21) it can be observed that for a dilute solid phase$s \to \infty$, and therefore $g_o \to 1$. In the limit when solid phase contact, $s \to 0$ and$g_o \to \infty$. For a one solid phase,

$$g_o = [1 - (\frac{\alpha_s}{\alpha_{s,max}})^{1/3}]^{-1} \tag{4.21}$$

4.4.1.6 Solid Shear Stresses

The solid shear stresses contain shear and bulk viscosities arising from particle momentum exchange due to translation and collision. A frictional component of viscosity can also be included to account for the viscous-plastic transition that occurs when particle of solid phase reach the maximum solid volume fraction. The collision and kinetics parts and the optional frictional part are added to give the solid shear viscosity as expressed below.

$$\mu_s = \mu_{s,col} + \mu_{s,kin} + \mu_{s,fr} \tag{4.22}$$

Collision Viscosity:

The collisional part of the shear viscosity is modeled as from Gidaspow et al. (1992) and Syamlal et al. (1993) as mentioned below:

$$\mu_{s,col} = \frac{4}{5}\alpha_s \rho_s d_s g_{o,ss}(1 + e_{ss})(\frac{\Theta_s}{\pi})^{1/2}\alpha_s \tag{4.23}$$

Kinetic Viscosity:

The kinetic part of the shear viscosity is modeled as from Syamlal et al. (1993)

$$\mu_{s,kin} = \frac{\alpha_s d_s \rho_s \sqrt{\Theta_s \pi}}{6(3 - e_{ss})}\left[1 + \frac{2}{5}(1 + e_{ss})(3e_{ss} - 1)\alpha_s g_{o,ss}\right] \tag{4.24}$$

Bulk Viscosity:

The bulk viscosity account for the resistance of the granular particle to compression and expansion. It has the following form (Lun et al. ,1984).

$$\lambda_s = \frac{4}{3}\alpha_s \rho_s d_s g_{o,ss}(1 + e_{ss})(\Theta_s/\pi)^{\frac{1}{2}} \tag{4.25}$$

Frictional Viscosity:

In dense flow at low shear, where the secondary volume fraction for a solid phase approaches the packing limit, the generation of stress is mainly due to friction between particles.

In the present work, Schaeffer's expression for frictional viscosity as mentioned below is considered.

$$\mu_{s.fr} = \frac{p_s \sin\phi}{2\sqrt{I_{2D}}} \tag{4.26}$$

where p_s is the solids pressure,ϕ is the angle of internal friction, and I_{2D} is the second invariant of the deviatoric stress tensor.

4.4.1.7 Granular Temperature

The granular temperature for the s[th] solids phase is proportional to the kinetic energy of random motion of particles. The transport equation derived from kinetic theory takes the following form.

$$\frac{3}{2}\left[\frac{\partial}{\partial t}(\rho_s\alpha_s\Theta_s) + \nabla.(\rho_s\alpha_s\vec{v}_s\Theta_s)\right] = \left(-p_s\bar{\bar{I}} + \bar{\bar{\tau}}_s\right):\nabla.\vec{v}_s + \nabla.\left(K_{\Theta_s}\nabla.\Theta_s\right) - \Upsilon_{\Theta_s} + \Phi_{ls} \tag{4.27}$$

Where

$\left(-p_s\bar{\bar{I}} + \bar{\bar{\tau}}_s\right):\nabla.\vec{v}_s$ = the generation of energy by solid stress tensor

$K_{\Theta_s}\nabla.\Theta_s$ = the diffusion of energy (K_{Θ_s} is the diffusion co-efficient)

Υ_{Θ_s} = the collisional dissipation of energy

Φ_{ls} = the energy exchange between the *l*[th] phase or solid phase and the s[th] solid phase

$K_{\Theta_s}.\nabla.\Theta_s$ describe the diffusive flux of granular energy. The diffusion co-efficient for granular energy, $K_{\Theta_s}$is given by

$$K_{\Theta_s} = \frac{15\,d_s\rho_s\alpha_s\sqrt{\Theta_s\pi}}{4(41-33\eta)}\left[1 + \frac{12}{5}\eta^2(4\eta-3)\alpha_s g_{0,ss} + \frac{16}{15\pi}(41-33\eta)\eta\alpha_s g_{0,ss}\right] \tag{4.28}$$

Where

$$\eta = \frac{1}{2}(1+e_{ss})$$

The collisional dissipation of energy,Y_{Θ_s}, represents the rate of energy dissipation within the s[th] solid phase due to collision between particles. This term is represented by the following expression:

$$\Upsilon_{\Theta_m} = \frac{12(1-e_{ss}^2)g_{0,ss}}{d_s\sqrt{\pi}}.\rho_s\alpha_s^2\Theta_s^{3/2} \tag{4.29}$$

The transfer of the kinetic energy of random fluctuations in particle velocity from the s[th] solid phase to the l[th] fluid or solid phase is represented by ϕ_{ls} which is written as

$$\phi_{ls} = -3K_{ls}\Theta_s \tag{4.30}$$

4.4.1.8 Turbulence Model

To describe the effect of turbulent fluctuations of velocities in a multiphase flow, large numbers of terms are to be modeled in the momentum equations and this make the modeling of turbulence in multiphase simulations extremely complex. There are three methods for modeling turbulence in multiphase flow. These are mixture turbulence model, dispersed turbulence model and turbulence model for each phase. In the present work dispersed turbulence model is applied.

K − ε Dispersed Model:

This model is applicable only when there is clearly one primary continuous phase and rest are dispersed dilute secondary phases. In this case, interparticle collisions are negligible and the dominant process in the random motion of the secondary phase is the influence of the primary phase turbulence. Fluctuating quantities of the secondary phases can therefore be defined in term of the mean characteristics of the primary phase and the ratio of the mean particle relaxation time and eddy-particle relaxation time.

Turbulence in the continuous phase:

The eddy viscosity model is used to calculate average fluctuation quantities. The Reynolds stress tensor for continuous phase, q takes the following form:

$$\bar{\bar{\tau}}_q'' = -\frac{2}{3}\left(\rho_p k_q + \rho_q v_{t,q}.\nabla.\vec{U}_q\right)\bar{\bar{I}} + \rho_q v_{t,q}\left(\nabla.\bar{\bar{U}}_q + \nabla.\vec{U}_q^T\right) \quad (4.31)$$

Where, $\vec{U}_q$ is the phase-weighted velocity.

The turbulent viscosity $\mu_{t,q}$ is written in term of the turbulent kinetic energy of phase q as follows: expression:

$$\mu_{t,q} = \rho_q C_\mu \frac{k_q^2}{\varepsilon_q} \quad (4.32)$$

The characteristic time of the energetic turbulence eddies is defined as:

$$\tau_{t,p} = \frac{3}{2} C_\mu \frac{k_q}{\varepsilon_q} \quad (4.33)$$

Where, $\varepsilon_q$is the dissipation rate and C_μ = 0.9.

The length scale of the turbulent eddies is written as:

$$L_{t,q} = \sqrt{\frac{3}{2}}\, C_\mu \frac{k_q^{3/2}}{\varepsilon_q} \quad (4.34)$$

Turbulent predictions are obtained from the modified $K-\varepsilon$ model as follows:

$$\frac{\partial}{\partial t}(\alpha_q \rho_q k_q) + \nabla.(\alpha_q \rho_q \vec{U}_q k_q) = \nabla.\left(\alpha_q \frac{\mu_{t,q}}{\sigma_k} \nabla k_q\right) + \alpha_q \rho_q \varepsilon_q + \alpha_q \rho_q \Pi_{k_q} \quad (4.35)$$

and

$$\frac{\partial}{\partial t}(\alpha_q \rho_q \varepsilon_q) + \nabla.(\alpha_q \rho_q \vec{U}_q k_q) = \nabla.\left(\alpha_q \frac{\mu_{t,q}}{\sigma_\varepsilon} \nabla \varepsilon_q\right) + \alpha_q \frac{\varepsilon_q}{k_q}(C_{1\varepsilon} G_{k,q} - C_{2\varepsilon} \rho_q \varepsilon_q) + \alpha_q \rho_q \Pi_{\varepsilon_q} \quad (4.36)$$

Here Π_{k_q} and Π_{ε_q} represent the influence the dispersed phase on the continuous phase q, and $G_{k,q}$ is production of turbulence kinetic energy.

The term Π_{k_q} is derived from the instantaneous equation of the continuous phase and takes the following form:

$$\Pi_{kq} = \sum_{p=1}^{M} \frac{k_{pq}}{\alpha_q \rho_q} \left(k_{pq} - 2k_q + \vec{v}_{pq}.\vec{v}_{dr}\right) \quad (4.37)$$

M represents the number of secondary phases.

Turbulence in the dispersed phase:

Time and length scale which characterize the motion are used to evaluate dispersion co-efficient correlation functions and the turbulent kinetic energy of each dispersed phase.

The characteristic relaxation time connected with inertial effects acting on a dispersed phase p is defined as:

$$\tau_{F,pq} = \alpha_p \rho_q K_{pq}^{-1} \left(\frac{\rho_p}{\rho_q} + C_v\right) \quad (4.38)$$

The Lagrangian integral time scale is calculated along the particle trajectories and is mainly affected by the crossing trajectories. This is defined as:

$$\tau_{t,pq} = \frac{\tau_{t.q}}{\sqrt{(1+C_\beta \xi^2}} \quad (4.39)$$

Where

$$\xi = \frac{|\vec{v}_{pq}|\tau_{t,q}}{L_{t,q}} \quad (4.40)$$

and

$$C_\beta = 1.8 - 1.35(\cos\theta)^2 \tag{4.41}$$

Where θ is the angle between the mean particle velocity and the mean relative velocity.
The ratio between these characteristic times is written as:

$$\eta_{pq} = \frac{\tau_{t,pq}}{\tau_{F,pq}} \tag{4.42}$$

Turbulence quantities for dispersed phase, p are written as:

$$k_p = k_q\left(\frac{b^2+\eta_{pq}}{1+\eta_{pq}}\right) \tag{4.43}$$

$$k_{pq} = 2k_q\left(\frac{b+\eta_{pq}}{1+\eta_{pq}}\right) \tag{4.44}$$

$$D_{t,pq} = \frac{1}{3}k_{pq}\tau_{t,pq} \tag{4.45}$$

$$D_p = D_{t,pq} + \left(\frac{2}{3}k_p - b\frac{1}{3}k_{pq}\right)\tau_{F,pq} \tag{4.46}$$

$$b = (1 + C_v)\left(\frac{\rho_p}{\rho_q} + C_v\right) \tag{4.47}$$

C_v = 0.5 is the added mass coefficient.

4.4.1.9 Species Transport Equations

The mixing and transport of chemical species are modeled by solving the conservation equations describing convection, diffusion, and reaction sources for each of the component species. The species transport equations are solved by predicting the local mass fraction of each species, Yi, through the solution of a convection-diffusion equation for i^{th} species. The species transport equation in general form is given as:

$$\frac{\partial}{\partial t}(\rho Y_i) + \nabla\cdot(\rho\vec{v}Y_i) = -\nabla\cdot\vec{J}_i + R_i + S_i \tag{4.48}$$

R_i = the net rate of production of species i by chemical reaction

S_i = the rate of creation by addition from the dispersed phase

An equation of this form will be solved for N-1 species where N is the total number of fluid phase chemical species present in the system. Since the mass fraction of the species must

sum to unity, the N^{th} mass fraction is determined as one minus the sum of the N-1 solved mass fractions, since the total mass fraction must sum to unity.

$\vec{J}_i$ is the diffusion flux of species i, which arises due to concentration gradients. Mass diffusion for laminar flows is given as:

$$\vec{J}_i = -\rho D_{i,m} \nabla Y_i \tag{4.49}$$

For turbulent flows, mass diffusion flux is given as

$$\vec{J}_i = -\left(\rho D_{i,m} + \frac{\mu_t}{Sc_t}\right) \nabla Y_i \tag{4.50}$$

Where Sc_t is the turbulent Schmidt number.

CHAPTER FIVE

HYDRODYNAMIC STUDY

CFD modelling for the hydrodynamic studies of fluidized bed gasifier has been carried out in this chapter. Before studying the details of reactions in different zones of the gasifier, it is essential to know the bed behaviour first such as identification and characterization of the flow regimes and structures in FBG. In the present work, a parameter study on a bubbling fluidised bed has been carried out. The effects of gas velocity and particle size on the flow dynamics have been studied.

5.1 Model and Simulation Method

ANSYS FLUENT.13.0 is used for simulation where 2D segregated first order implicit unsteady solver is used for multiphase calculations. Standard k-ε dispersed Eulerian multiphase model with standard wall functions are used. Gas is taken as continuous phase while binary mixtures of solid particles are taken as dispersed phase. Interphase interaction formulations used are of Solid–Solid (Syamlal-Obrien-symmetric) and Solid-Gas (Gidaspow) types. Inert material sand has been used as the bed material in the present work. Biomass (Rice husk) has been considered as the feed sample in FBG. Air is used as the fluidizing medium which is supplied from bottom of the FBG.

5.1.1 Assumptions Made

For carrying out simulation on any process, certain assumptions are required for initializing the computational work. In the present case also, certain assumptions have been considered. In the present work, isothermal non-reactive, unsteady state gas-solid system are considered as basic assumptions in cold model FB gasifier unit. Eulerian multi-fluid model is adopted where both gas and solid phases are treated as continua, inter-penetrating and interacting with each other everywhere in the computational domain. The single pressure field is assumed to be shared for all three phases, in proportion to their volume fractions. Gas phase has been modelled with k-ε turbulent model and solid phases have been modelled with the kinetic theory of granular flow. The motion of each phase is governed by their mass and momentum conservation equations as described in chapter 4.

5.1.2 Geometry and Mesh

The reactor used for the bubbling fluidised bed is based on the experimental set up used in laboratory. Fig. 1(a) shows geometry of the reactor with its dimensions. The bubbling bed zone has inner diameters of 0.15m and height of 1m. The free board area has inner diameters of 0.3m

and height of 0.8m. The geometry is generated by using commercial software GAMBIT. After geometry creation, a uniform mesh has been generated. Structured meshing method is used for meshing the geometry. In this study, total of 16,346 cells and16782 numbers of nodes are employed for simulating Fluidized Bed Gasifier.

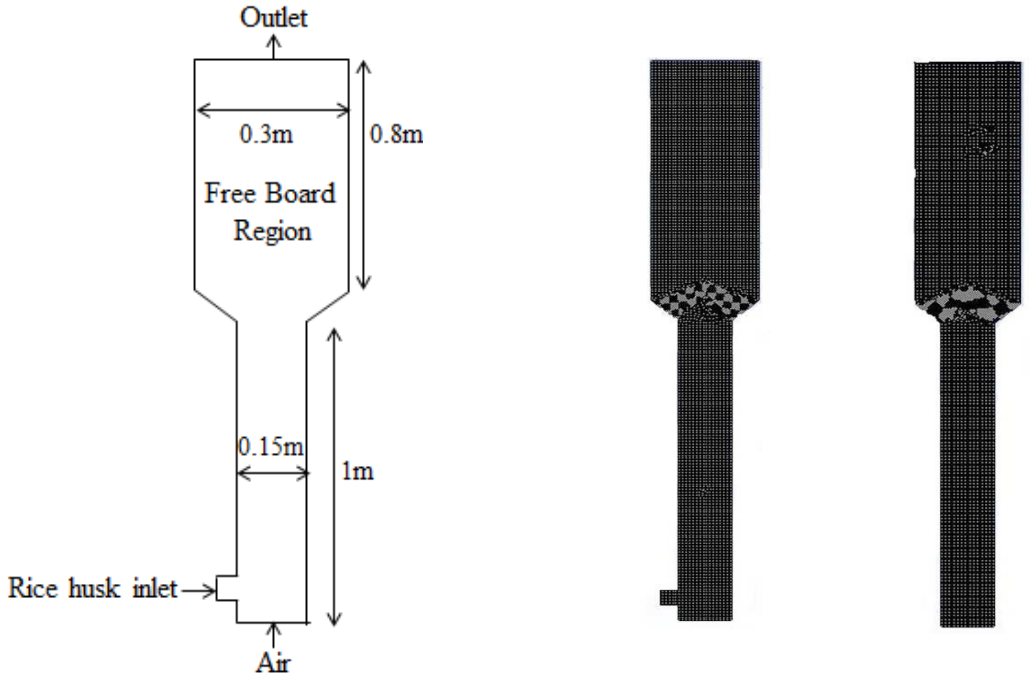

Fig.5. 1(a) Geometry of fluidized bed (b) 2-D Mesh 1 (c) 2-D Mesh 2

5.1.3 Phases and Materials

The case is simulated using three phases, which enter the gasifier through boundary conditions and interact by exchanging mass and momentum. These three phases are:

1. Gas phase: This is the Primary phase. The gas phase is used for simulating both the air inlet and the product gas outlet.
2. Sand: It is the secondary phase. This phase represents the fluidizing bed material which is sand in this study. The sand is modelled granular and inert with a constant size of 385 μm and density 2650 kg/m^3, belonging to Geldart B group.
3. Rice husk: It is also considered as secondary phase. This phase simulates the fuel inlet of the gasifier. It is considered to be a granular phase.

Table 5.1: List of used parameters with the name of models

Parameter	Model in (Fluent 13.0)
Solid viscosity	Gidaspow
Solid bulk viscosity	Lun et al.
Frictional viscosity	Scheaffer
Solid pressure	Lun et al.
Radial distribution function	Lun et al.
Drag law (gas-solid)	Gidaspow
Drag law (solid-solid)	Syamlal and O'Brien symmetric

5.1.4 Boundary and Initial Conditions

The initial and boundary conditions for the gas phase and solid phase simulations are used for the geometry shown in Fig. 5.1 (a). The simulation is assumed to be non-reactive and a cold flow fluidization system therefore the operating conditions for the present case are assumed to be 300K temperature and 1 atmpressure.

Figure 5.1 (a) shows the full FB gasifier geometry where both sand and rice husk are initially in static condition inside the fluidized bed column with 0.1 m initial static bed height. Thus solid particles velocity is set at zero and the inlet gas velocity at the bottom of FB is assumed to be uniform along the axial direction. The pressure is not specified at the inlet because of the incompressible gas phase assumption (relatively low pressure drop system). At the outlet, only pressure boundary condition is specified. The boundary condition at the walls is assumed such that the tangential and normal velocities are zero. Such conditions are known as no-slip boundary conditions.

Table 5.2: Simulation model parameters used for gas and solid flow in a FBG

Property	Value	unit
Gas density(air)	1.2	kg/m^3
Gas viscosity	$1.7894*10^{-5}$	Pa.s
Biomass density	426	kg/m^3
Biomass particle diameter	856, 530	μm

Density of inert solid(sand)	2650	kg/m^3
Diameter of sand	385	μm
Superficial gas velocity	0.2	m/s
Static bed height	0.1	m
Biomass inlet velocity	0.005	m/s
Restitution coefficient, e	0.9	-

5.1.5 Solution Techniques

The Phase Coupled SIMPLE method has been chosen for pressure–velocity coupling. The second-order upwind scheme has been used for discretization of momentum, turbulence kinetic energy and turbulence dissipation rate and the first-order upwind scheme has been used for discretization of volume-fraction equations. The time step of size =0.001s is taken for the solution to converge. Under relaxation factors for different flow quantities are mentioned in table 5.3.

Table 5.3: Under relaxation factors for different flow quantities

Variable	Relaxtion Factor
Pressure	0.5
Density	1
Body Force	1
Momentum	0.2
Volume Fraction	0.4
Granular Temperature	0.2
Energy	0.8

5.2 Results and Discussion

5.2.1 Contours of Solid Volume Fraction

The contour plots of volume fraction of rice husk, sand and air with air inlet velocity of 0.05m/s are shown in Fig 5.2 and 5.3. It is observed that the bed begins to expand at this velocity but the height of the bed remaining same as for a fixed bed. The particles move about slightly, but only

on a small scale and the particles just start to exhibit fluid-like behaviour. Thus the upward drag on the solid packing is equal to the weight of the packing at this condition.

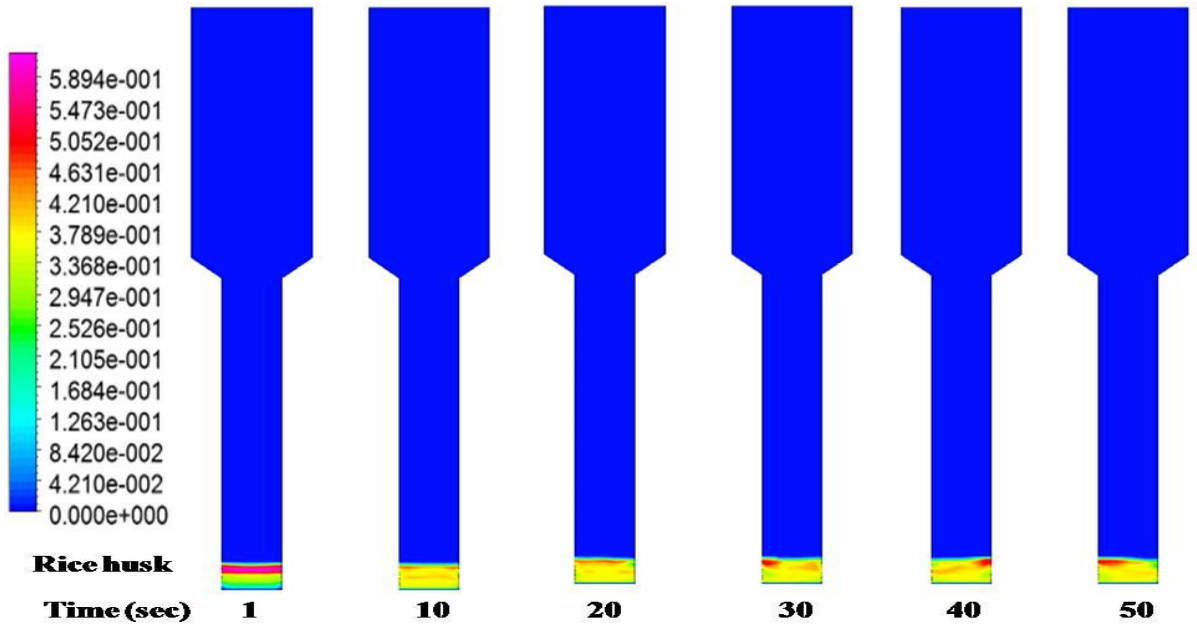

Fig. 5.2: Contour plot of volume fraction against time for rice husk at air velocity of 0.05m/s for initial static bed height of 0.1m

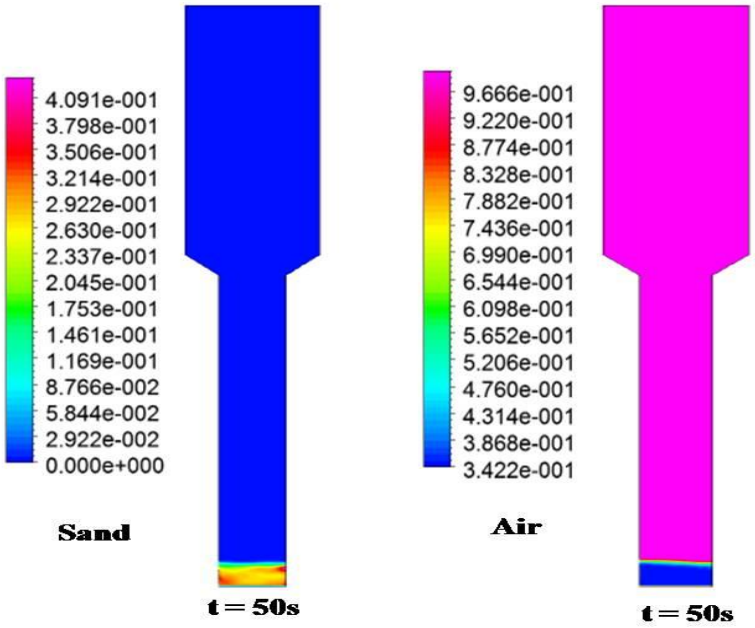

Fig. 5.3: Contour plot of volume fraction of sand and air at air velocity of 0.05m/s for initial static bed height of 0.1m

The contour plots of the rice husk and sand with an inlet velocity of 0.2 m/s have been shown in Fig.5.4 and 5.5 respectively. It is observed from Fig.5.4 that bubbles are formed only within the static bed height without any noticeable bed expansion. The reason may be attributed to the fact that bubbling occurs at the surface only. In other words, solids in the bottom section of the bed are in pneumatic transport while fluidization in the upper section is in freely bubbling state.

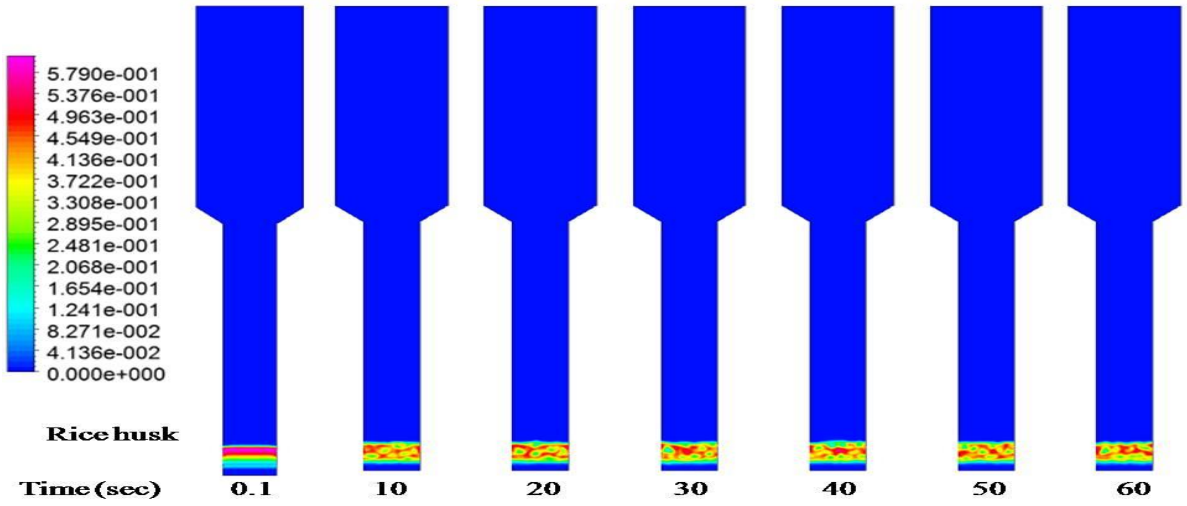

Fig. 5.4: Contour plot of volume fraction against time for rice husk at air velocity of 0.2m/s for initial static bed height of 0.1m

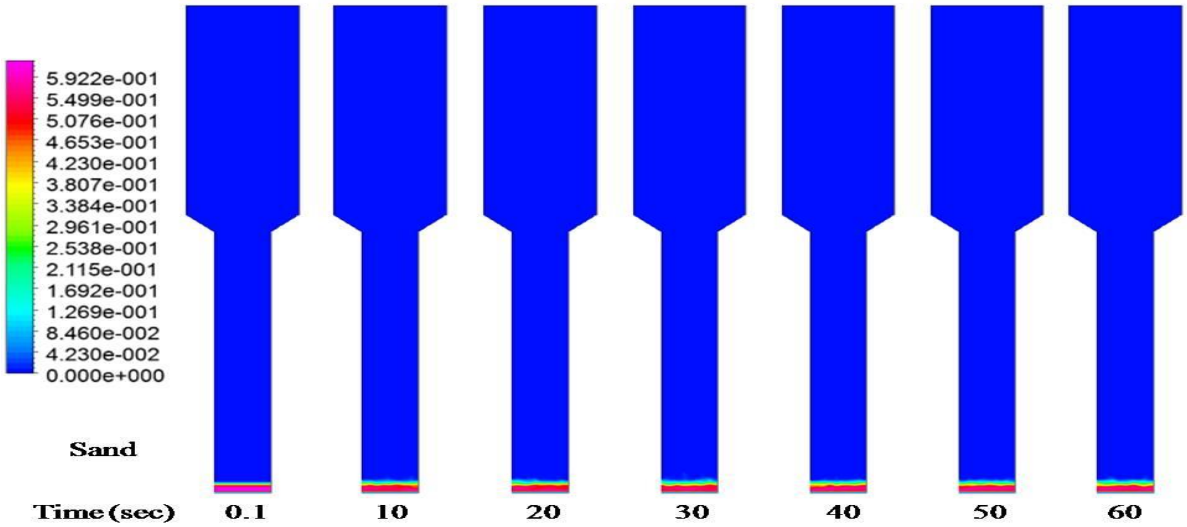

Fig. 5.5: Contour plot of volume fraction against time for sand at air velocity of 0.2m/s for initial static bed height of 0.1m

Fig.5.6 shows the variation in the bed profile with time for rice husk at air velocity of 0.5m/s. The contour plot has been plotted with time step of 10secs. While simulating the fluidized bed, it is observed that the bed profile changes with time. But after some time no significant change is observed in the bed profile. This indicates that the fluidized bed has come to a quasi-steady state. The contour plot in Fig.5.6 shows higher solid volume fractions along the walls compared to the core region. This may be due to the segregative tendencies of the particles towards the walls or gulf streaming. Thus the solid particles slide down along the wall of the reactor without too much resistance from the upward gas flow.

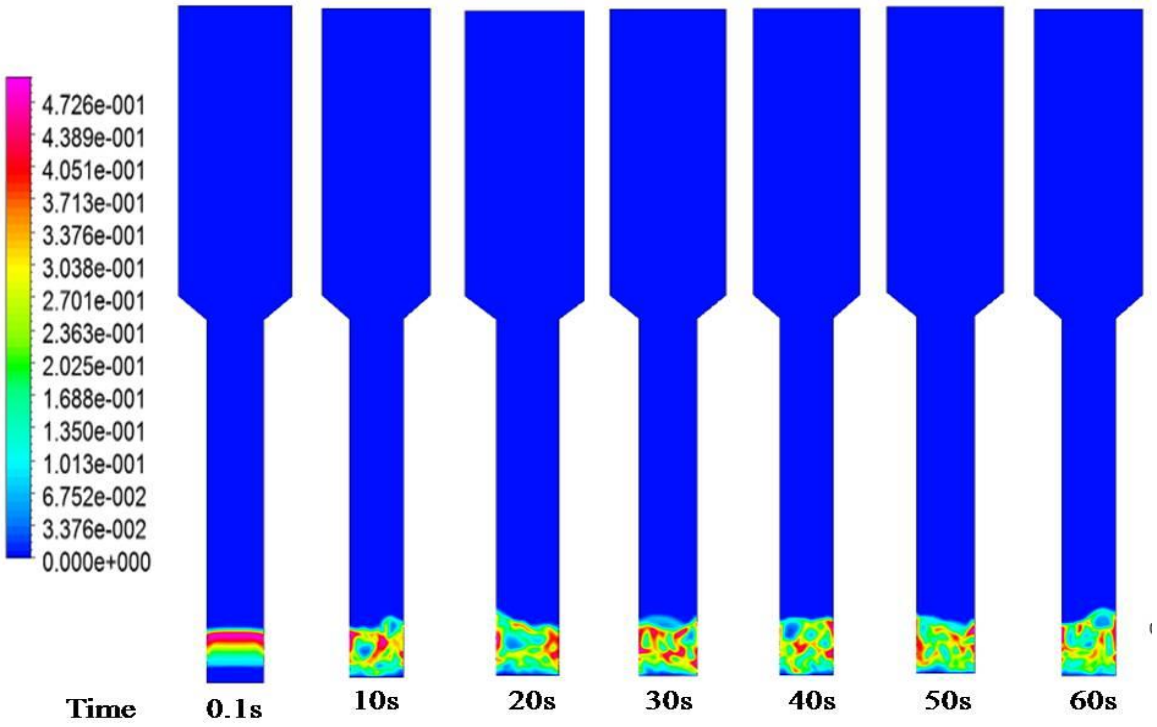

Fig. 5.6: Contour plot of volume fraction of rice husk at air velocity of 0.5m/sec with respect of time for initial static bed height of 0.1m

Fig.5.7 shows the contours of volume fractions of rice husk, sand and air obtained at air velocity of 0.7 m/s for initial static bed height 0.1m in 2-D fluidized bed after the quasi steady state is achieved. The colour scale given to the left of each contours gives the value of volume fractions corresponding to any particular colour. The contours for rice husk and sand illustrates that bed is in fluidized condition. The contour for air illustrates that volume fraction of the gas is less in fluidized section than the solid particles

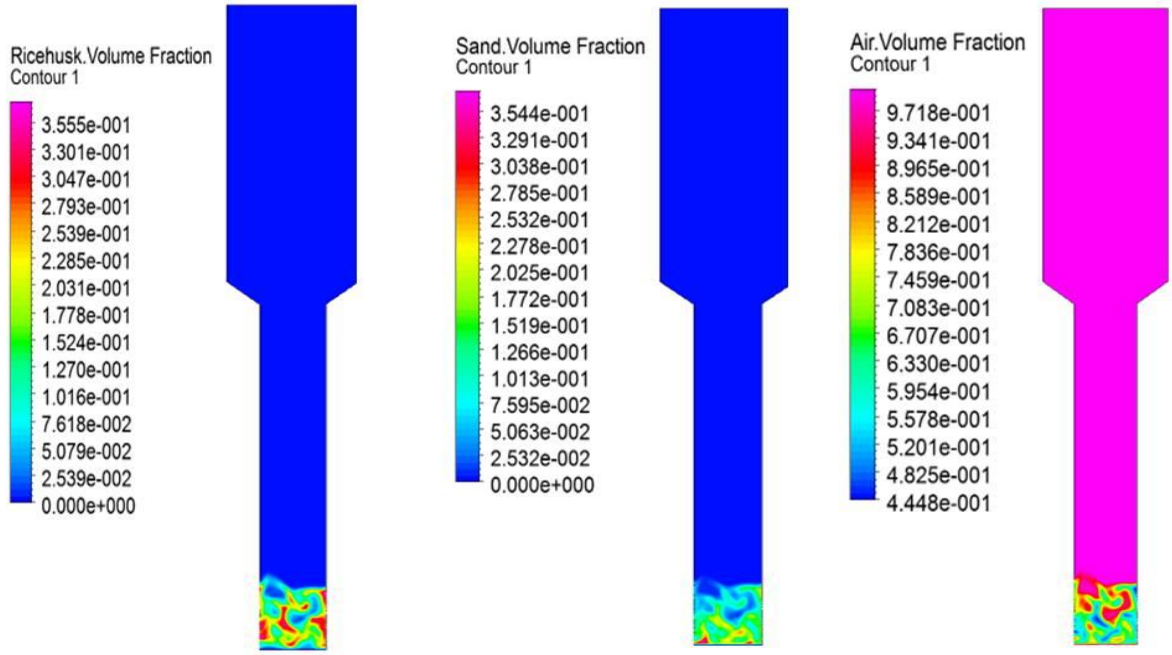

Fig. 5.7: Contour plot of volume fraction for rice husk, sand and air at air velocity 0.7m/s

5.2.2 Phase Velocity

The velocity vectors show magnitude of velocity with direction and thus helpful to determine the flow pattern in fluidized bed. The velocity vectors of rice husk, sand and air in the column obtained after the quasi steady state at air velocity of 0.7 m/s with initial static bed height of 0.1 m are shown in Fig.5.8 and 5.9.

From velocity vector of solid phase (Fig.5.8), it is observed that there is vigorous movement of solid particles throughout the bed implying that the velocity at the bottom is less. In the central region of the bed, direction of velocity near the wall is observed to be downwards while that in the region away from wall is upwards. In the upper part of fluidizing section there is circulatory motion/ downward motion of the solid particles near the wall and upward motion in the central region of the bed. The velocity vector of gas phase in the column (Fig.5.9) indicates that there is an upward flow throughout the column which implies that velocity of air is very less within the bed compared to that in remaining part of the column. This is due to very small volume fraction of air within the bed compared to solids in that region. In the upper section of the column, air velocity is high thus it carries air bubbles but in the lower section of the column solid particles obstruct the movement of bubbles thereby reduces air velocity.

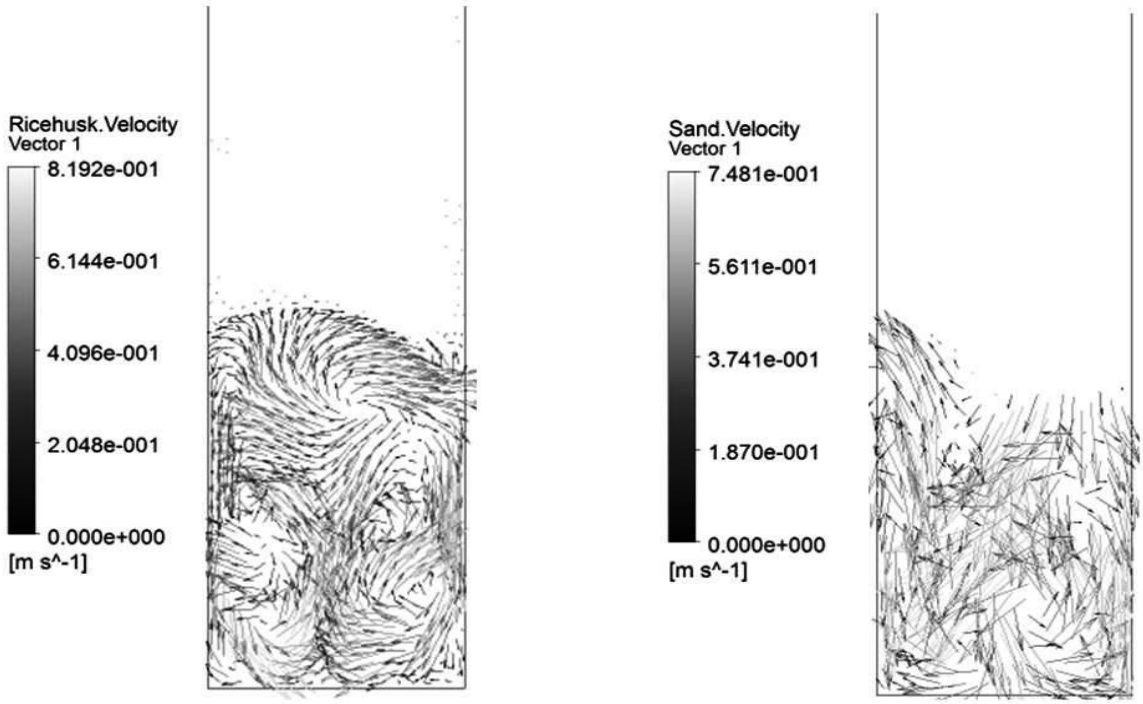

Fig. 5.8: Velocity vector of rice husk and sand at air velocity 0.7m/s

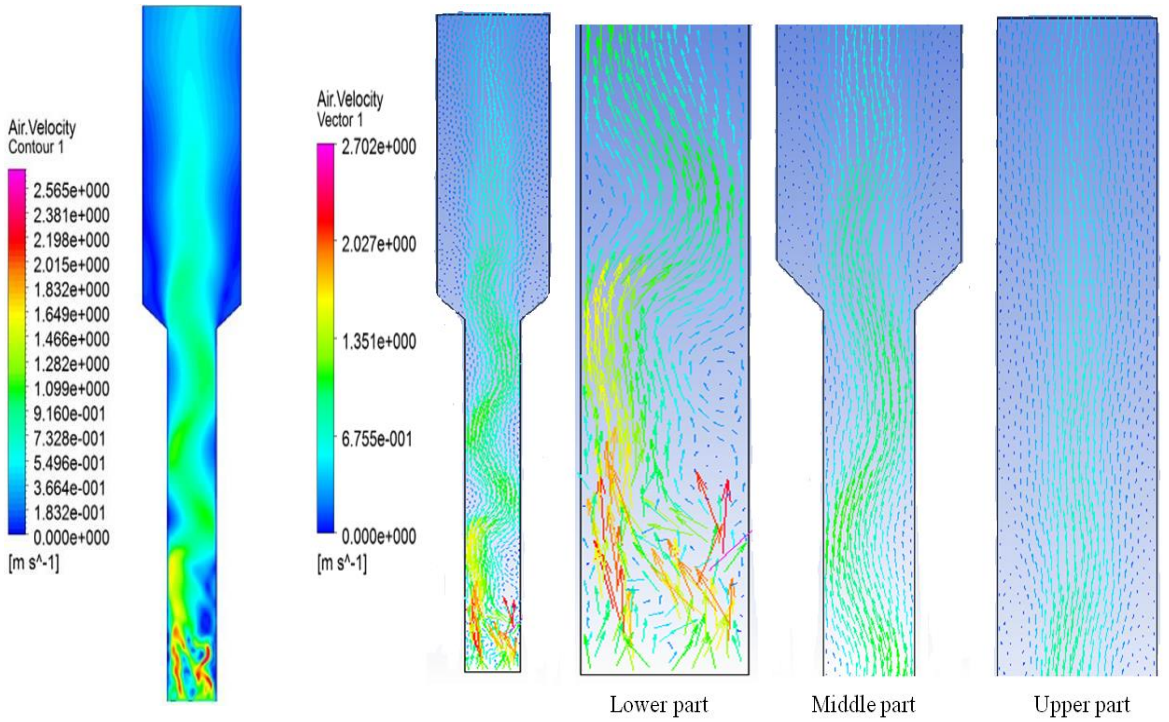

Fig. 5.9: Velocity contour and vector of air at air velocity 0.7m/s

5.2.3 Particle Distribution

Fig. 5.10 illustrates radial variation of solid concentration at different bed heights at air velocity 0.7m/s which shows higher particle volume fractions along the walls compared to the core region. The result confirms that the solid volume fraction is not symmetrical. According to the axial solid volume concentration profile (Fig. 5.10) the riser is axially divided into the lower zone and the upper zone. The lower region of FB riser is denser than the upper-dilute region even though the solids mainly accumulate in both sides the wall for 2D model. The computed time-averaged volume fraction of rice husk and sand particles for a bed height of 0.15m and a gas velocity of 0.5 m/s are compared (Fig. 5.11). The volume fraction of particles is observed to be lower in the central region than the region near the wall. From the simulation result as shown in the figures, the hydrodynamic model is able to describe quantitatively the accumulation of solids near the wall. Solid concentrations appear flat in the central region and increase towards the wall. This is due to the segregative tendencies of the particles towards the walls.

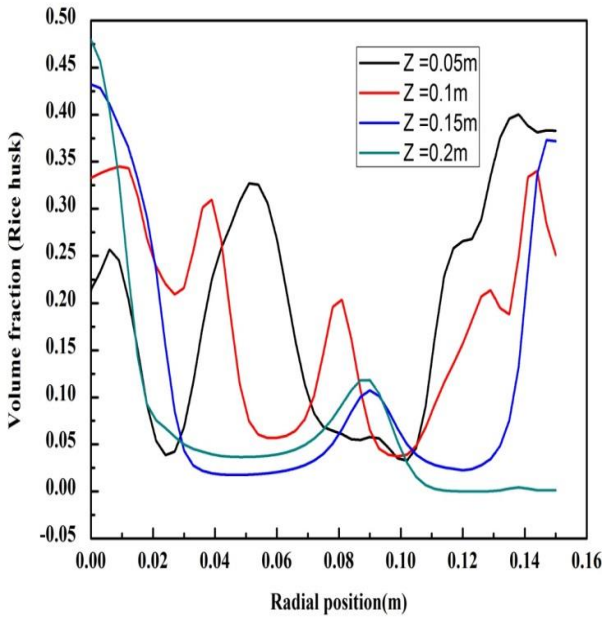

Fig. 5.10: rice husk particle concentration against the radial position for different bed heights at air inlet velocity of 0.7m/s

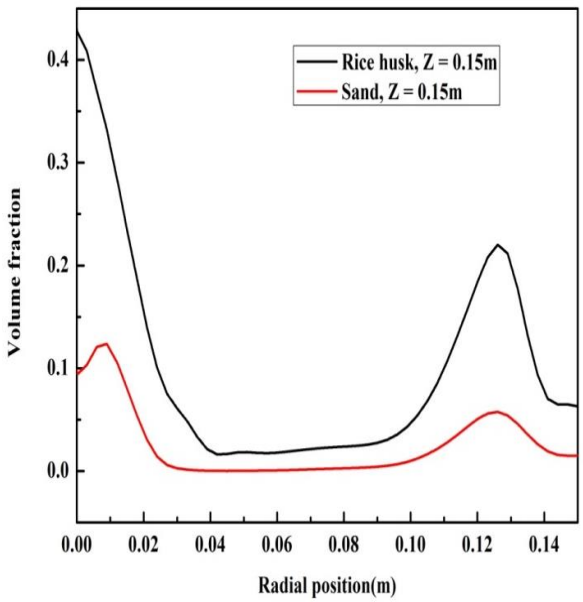

Fig. 5.11: Comparison of distributions of rice husk and sand at air velocity 0.5m/s

Fig.5.12. shows the plot of axial velocity of solid particles inside the 2-D fluidized bed model at gas velocity 0.7 m/s after quasi-steady state is reached. The velocity profiles across radial direction at different height (i.e. 0.05 m, 0.3 m, 0.5 m and 0.7m) of the fluidized section are plotted. It is observed that axial solid velocity is less in the lower section of the fluidized section and increases as move toward the higher section and attain maximum velocity. This occurs because of increased velocity of gas phases with the bed height. Solid velocities near wall are decreases and this may lead to the back accumulation of particles.

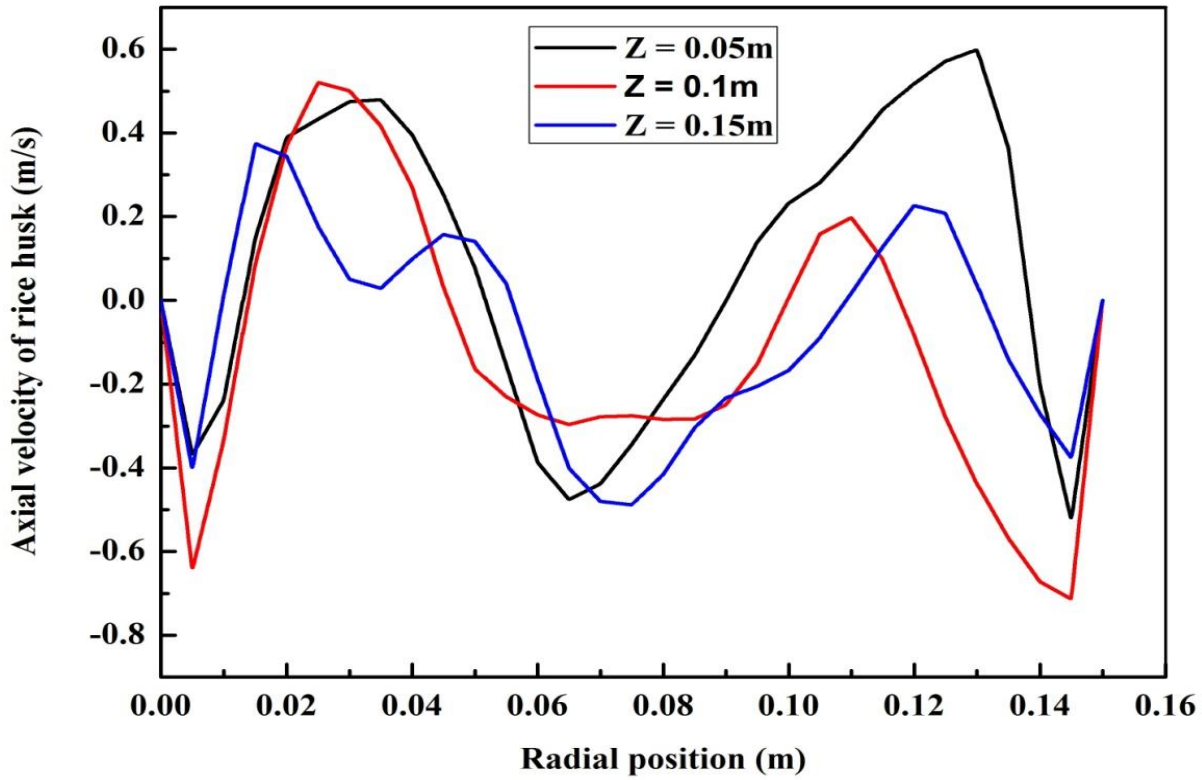

Fig.5.12: Time-average axial solids velocity distribution along the radial direction at V =0.7 m/s for [Z=0.05 m, Z=0.1 m, Z= 0.15 m]

5.2.4 The Influence of Particle Size

Fig.s 5.13 and 5.14 show the particle volume fraction distributions of two different particle sizes (856 μm and 530 μm) at the superficial gas velocity of 0.7 m/s. The volume fraction of particles increases towards the wall region. It is observed that the volume fraction of smaller particles is higher in the upper region (i.e. z=0.1m, 0.15 m) than that in the lower portion (i.e. z=0.05 m) of the riser. However the volume fraction of biger particles is found to be lower in the upper region than that in the lower portion of the riser.

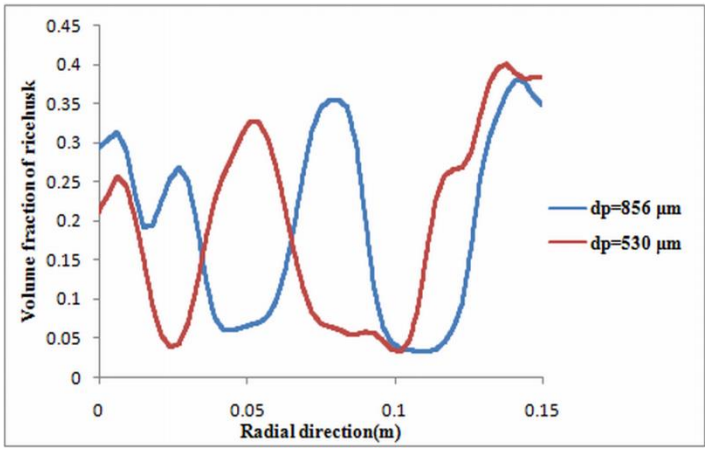

Fig. 5.13: Comparison of distribution of solid concentration for two different particle sizes at a height of 0.05m at air velocity 0.7m/s

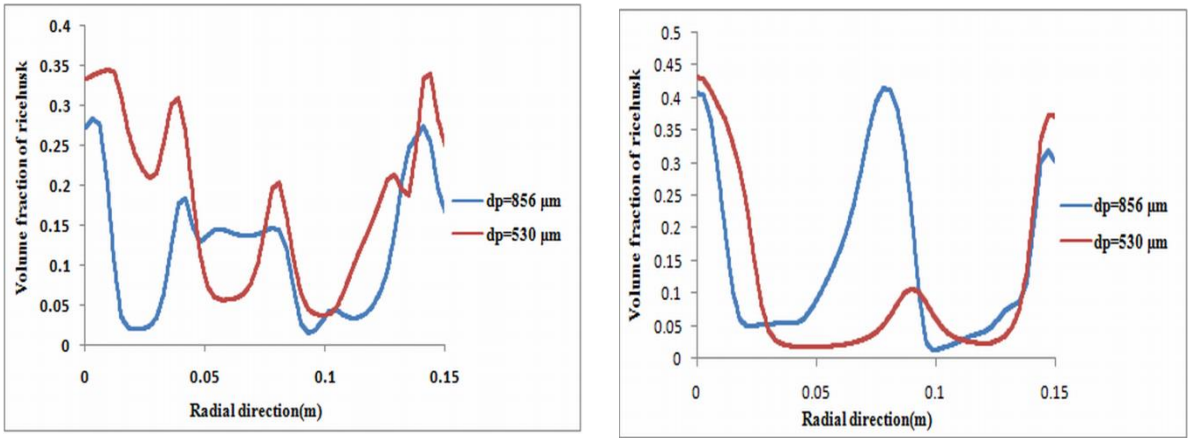

Fig. 5.14: Comparison of distribution of solid concentrations for two different particle sizes at a height of 0.1 and 0.15m at air velocity 0.7m/s

5.2.5 Bed Expansion Ratio

It is observed that the bed expansion ratio for two different particle sizes at various air velocities increases (Fig.5.15). It is further observed that the bed expansion decreases with particle size. This may be due to the requirement of higher drag to expand the bigger size particles than the lower sized particles thereby causing less expansion with bigger sized particles.

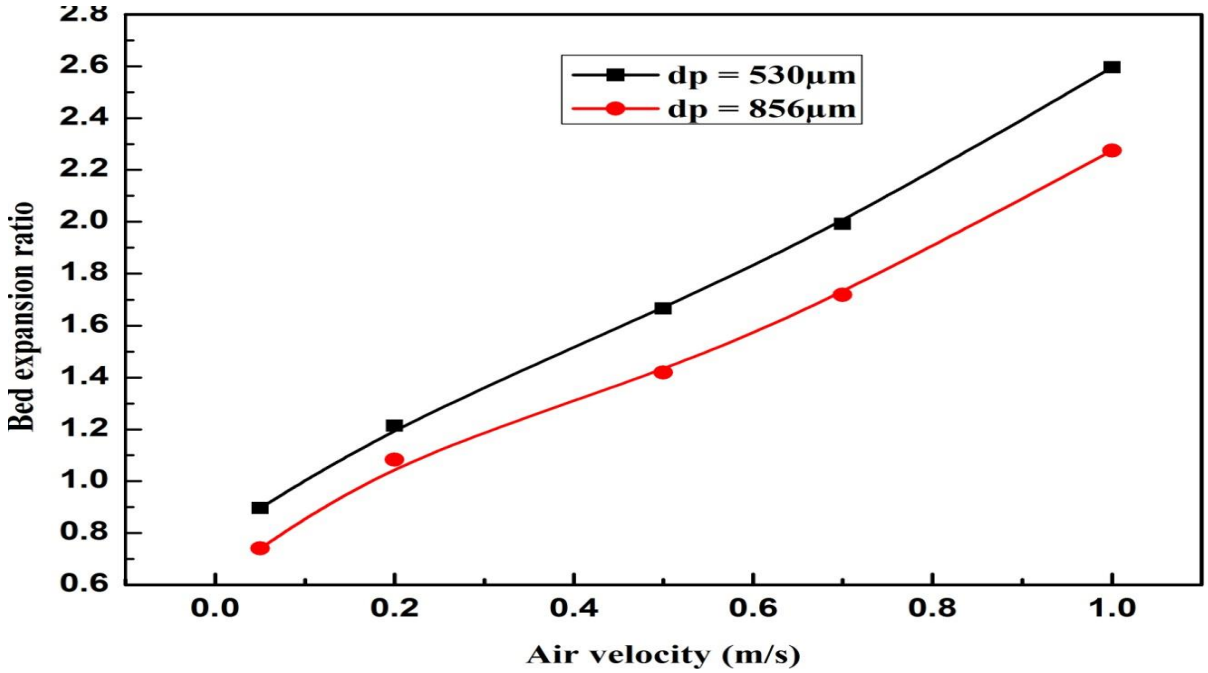

Fig. 5.15: Comparison of bed expansion ratios for two different sizes

5.2.6 Bed Pressure Drop

The axial pressure drop in a fluidized bed varies from higher value at the bottom of the bed to zero value at the top of the column. The bed pressure drop can be determined from the difference of pressure at the inlet and outlet. Fig.5.16 shows the contours of statics gauge pressure. It is evident from the figure that the pressure is higher at the inlet and gradually decreases and became zero at the outlet.

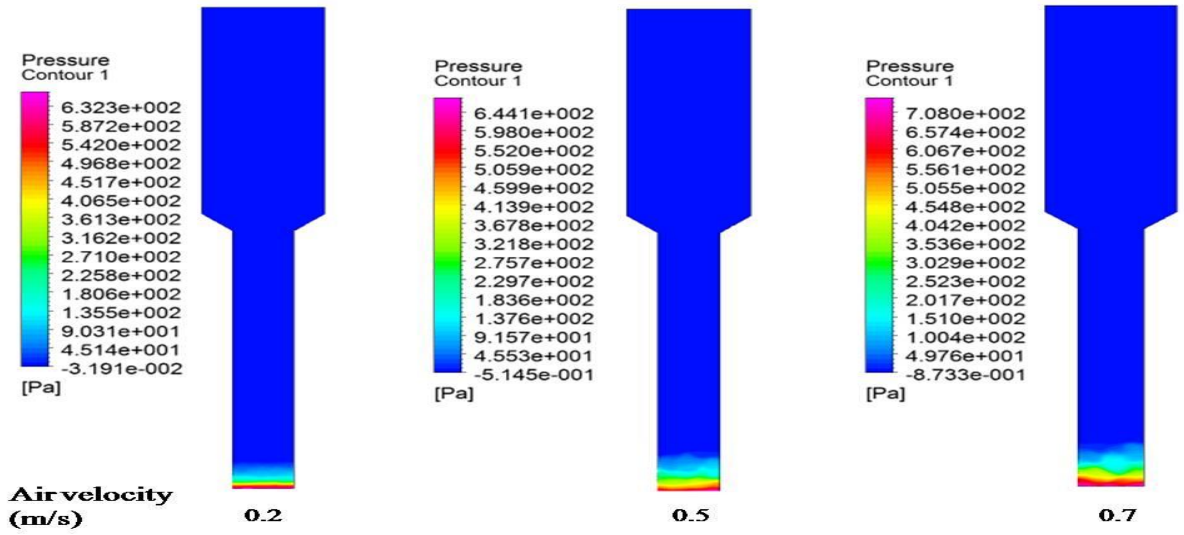

Fig.5.16: Contour of bed pressure drop against air velocity for the fluidized bed

5.2.7 Effects of Inlet Velocities

The volume fraction distribution for the particles using the Gidaspow model with four inlet velocities, i.e., 0.7 m/s, 0.1 m/s, 1.8 m/s and 2 m/s, are shown in Fig. 5.17(a-d) for particles with a diameter of 530 µm. If the gas velocity does not exceed V_t the particles fall back down to the particle bed. This is referred to as a bubbling bed and is shown in Fig. 5.17 (a) (b). Exceeding V_t means the suspended particles can be carried with the gas phase and continue up the riser. This fast fluidization state has been shown in Fig. 5.17 (c) (d).

The contour plots of Fig.5.17 (a) (b) show bubbles increasing in size and distorting with increasing height. This is due to the coalescence of the bubbles with smaller bubbles rising from the base of the reactor. As the velocity increases, the bubble sizes increase and the solid-gas mixture appears more dilute particularly towards the top of the bed. The solids descend to the base of the reactor as the solids and gas compromise.

The fast fluidizing states in Fig. 5.17 (c) (d) show very dilute distributions in comparison to the bubbling models. The particle volume fraction and particle velocity are shown in Fig. 5.17 (c) at gas velocity i.e 1.8m/s which is only slightly lower than the terminal velocity. Increasing the gas velocity allows for a faster flow of gas to push the collection particles higher up the bed. Fig.5.17 (d) shows the particle volume fraction and particle velocity at gas velocity 2m/s. So terminal velocity in the present study is found to be approximately 1.9m/s.

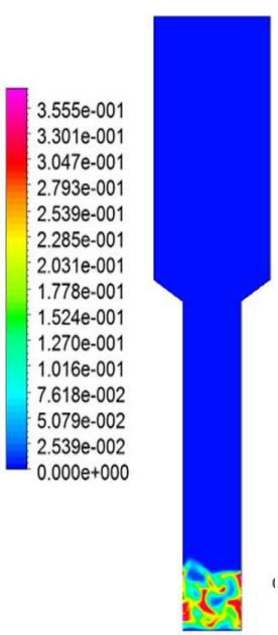

(a)

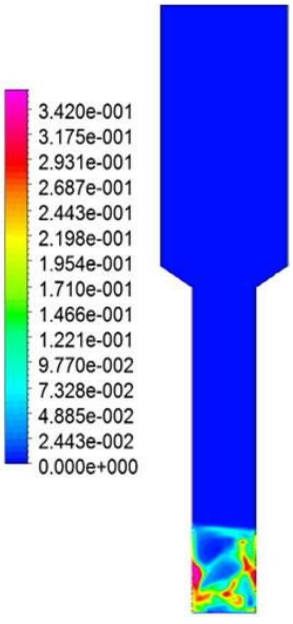

(b)

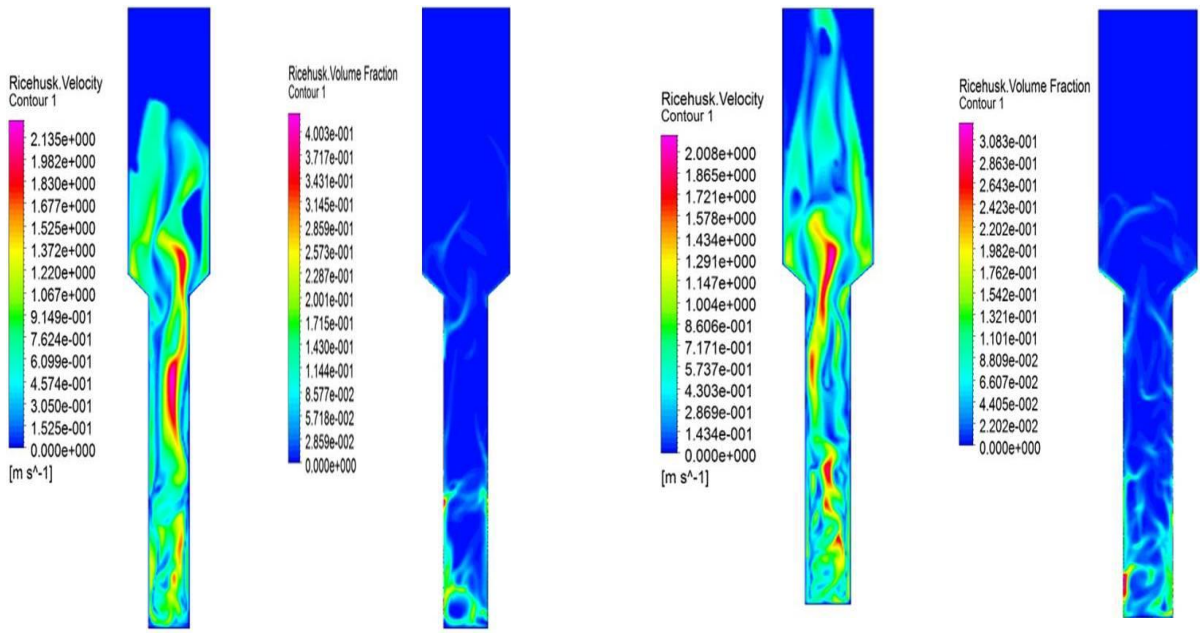

(c) (d)

Figure 5.17: Particle volume fraction and velocity vector for d_p = 530 µm a) V = 0.7 m/s, b) V = 1 m/s, c) V = 1.8 m/s d) V = 2 m/s.

CHAPTER SIX

REACTION MODELLING

This chapter incorporates reaction kinetics into an Eulerian-Eulerian model of a bubbling fluidized bed biomass gasifier. It is planned to establish a simulation model to study thermal flow and gasification process using a fluidized bed gasifier by Eulerain multi-phase approach. This chapter is categorized in three different sections as given below.

- Case 1: Thermo-flow behavior with solid (no reactions).
- Case-2: Homogeneous reaction (no solids).
- Case-3: Heterogeneous reaction (gas-solid) in the gasifier with volatiles (complete simulation).

The geometry and mesh used for the present study in this chapter are shown in Fig 5.1.

6.1 Case 1: Thermal-flow Behavior with Solids (No Reactions)

This case analyses the thermal-flow behavior with particles as well as the fluidization in the geometry. Sand and rice husk particles are patched up to a static bed height 0.1m. The air enters at a velocity of 0.7 m/s at 673 K and flows through the bed. All the other boundary conditions and solution techniques used in this study are the same as taken for previous hydrodynamic study in chapter five. The simulation model parameters as mentioned in Table 5.2 have been used for the present study.

6.1.1 Results and Discussion

The particle velocity field versus air velocity field has been shown in Figure 6.1. It can be clearly seen that all air streams move upward whereas particles circulate within the fluidized bed in the bottom part of the domain. At 0.7 m/s inlet air velocity, no particles are seen in the upper part of the domain. A sequence of volume fraction distributions of rice husk are shown in Fig.6 .2 at different seconds.

Bubbles are formed above the inlet due to the fast supply of air at a rate of 0.7 m/s. Then bubbles continue to rise towards the top of the bed along the wall. The bubbles also appears to elongated and circle back round towards the walls. This indicates the solid particles in the bed move in a circular motion thereby influencing and distorting the bubble back towards the wall. This is more clearly evident in Fig. 6.1 which displays the particle velocity vectors. Since no reactions are simulated in this case, the temperature inside the domain is gradually increases with time and after some time it becomes uniform throughout the bed (fig.6.3).

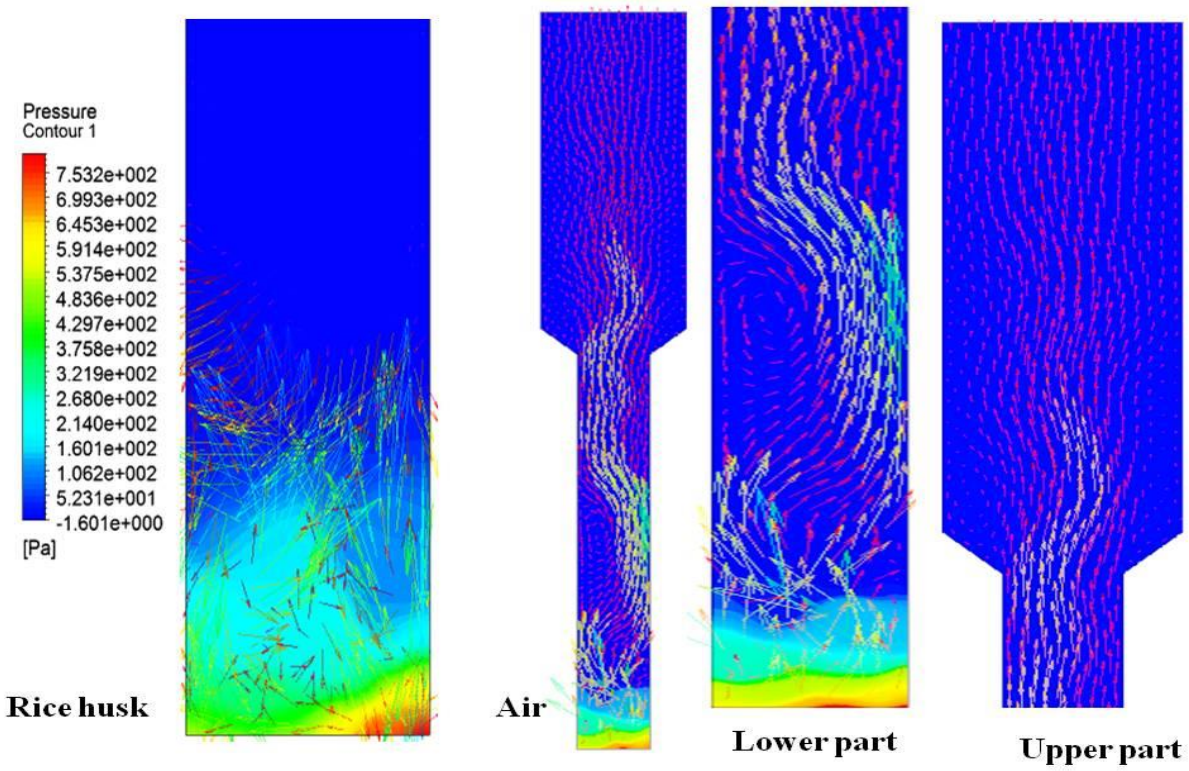

Fig. 6.1: Velocity vector plots for (a) rice husk and (b) colored by static pressure (Pascal) for Case 1

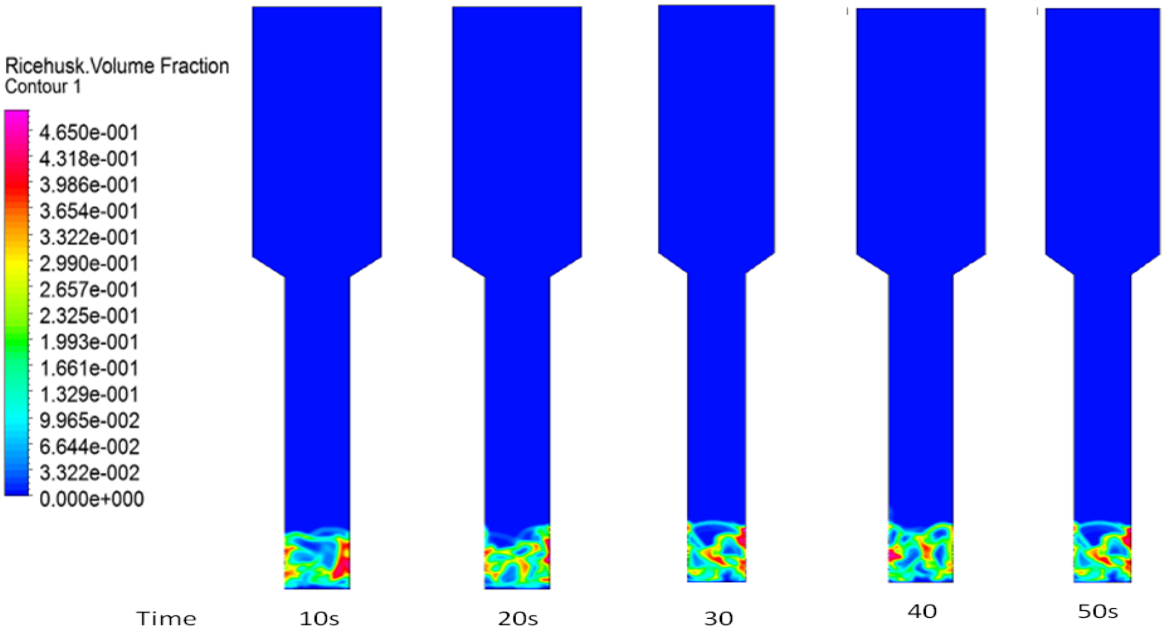

Fig. 6.2: Distribution of volume fraction of rice husk with time at air velocity 0.7m/s

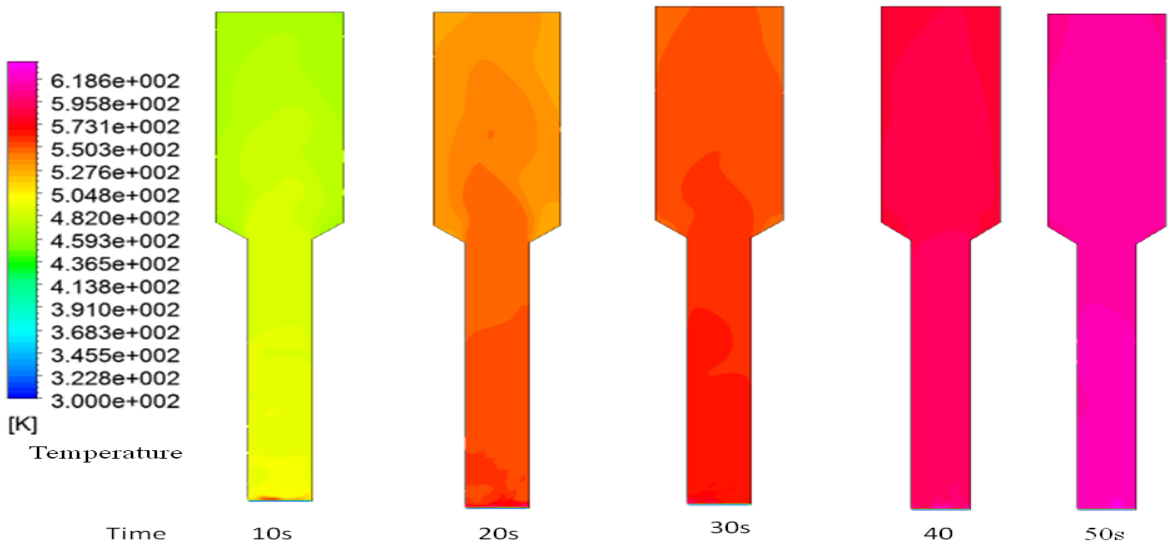

Fig. 6.3: Temperature profile at different time intervals inside the fluidized bed

6.2 CASE 2: Instantaneous Gasification Model or Homogenous Reaction (No Solids)

6.2.1 Problem Statement

This case investigates the adiabatic flame temperature and distribution of gas mass fraction by introducing the following five global gasification reactions (R6.1 to R6.5) together in the geometry. The mass weighted average of temperature and mass fraction of product gas are verified under a thermal equilibrium condition.

The Global Gasification Reactions are modeled as:

$$C(s) + \tfrac{1}{2} O_2 \rightarrow CO \quad (6.1)$$

$$C(s) + CO_2 \rightarrow 2CO \quad (6.2)$$

$$C(s) + H_2O\ (g) \rightarrow CO + H_2 \quad (6.3)$$

$$CO + \tfrac{1}{2} O_2 \rightarrow CO_2 \quad (6.4)$$

$$CO + H_2O\ (g) \rightarrow CO_2 + H_2 \quad (6.5)$$

For the single phase simulation, all these above reactions are treated as homogeneous reactions (i.e. Carbon, C(s) is treated as "gas" for homogeneous reaction). This is a necessary stepping stone to gain confidence with the modeling before considering heterogeneous reaction calculation.

6.2.2 Boundary and Initial Conditions

In order to obtain a well-posed system of equation, reasonable boundary conditions for the computational domain have to be implemented. At inlet velocity and temperature of the air and mass fraction of the species are specified. At outlet pressure boundary condition is specified. No slip boundary condition is specified at the wall.

Table 6.1 List of boundary conditions and composition of species

Parameters	Value
Gas velocity (m/s)	0.7
Gas inlet temperature(^{0}C)	600,700,800,1000
Operating pressure (Pascal)	101325
Mass Fraction at Inlet	
C	0.2046
H_2O	0.0734
N_2	0.77
O_2	0.23

6.2.3 Solution Techniques

In fluent, solver is set as segregated which solves the equation individually. Here pressure based solver is used. The species transport model is considered. Eddy dissipation model is used to predict the reaction rate. The discretization scheme for momentum, energy and species all have been taken as second order upwind and Quick scheme is used for solid and gas phase volume fraction. Under relaxation factors for different flow quantities are mentioned in table 6.2. The convergence criterion for continuity, velocity and species is considered as 0.001.

Table 6.2 Under relaxation factors for different flow quantities

Variable	Relaxtion Factor
Pressure	0.5
Density	1
Body Force	1
Momentum	0.2
Volume Fraction	0.4
Granular Temperature	0.2
Energy	0.8
Species	1

6.2.4 Results and Discussion

The gaseous mass fraction distributions within the reactor for instantaneous gasification model are shown in Fig.6.4. The species CO, H_2 and CO_2 show larger mass fraction at the base of the gasifier. These gaseous species decrease with height as they are consumed by further reactions. Gasification takes place and completes very fast within the gasifier as all the reactants (C, O_2, steam) are quickly consumed giving mass fraction values nearly equal to zero. All the products reach quickly their maximum amounts (CO, CO_2, and H_2).

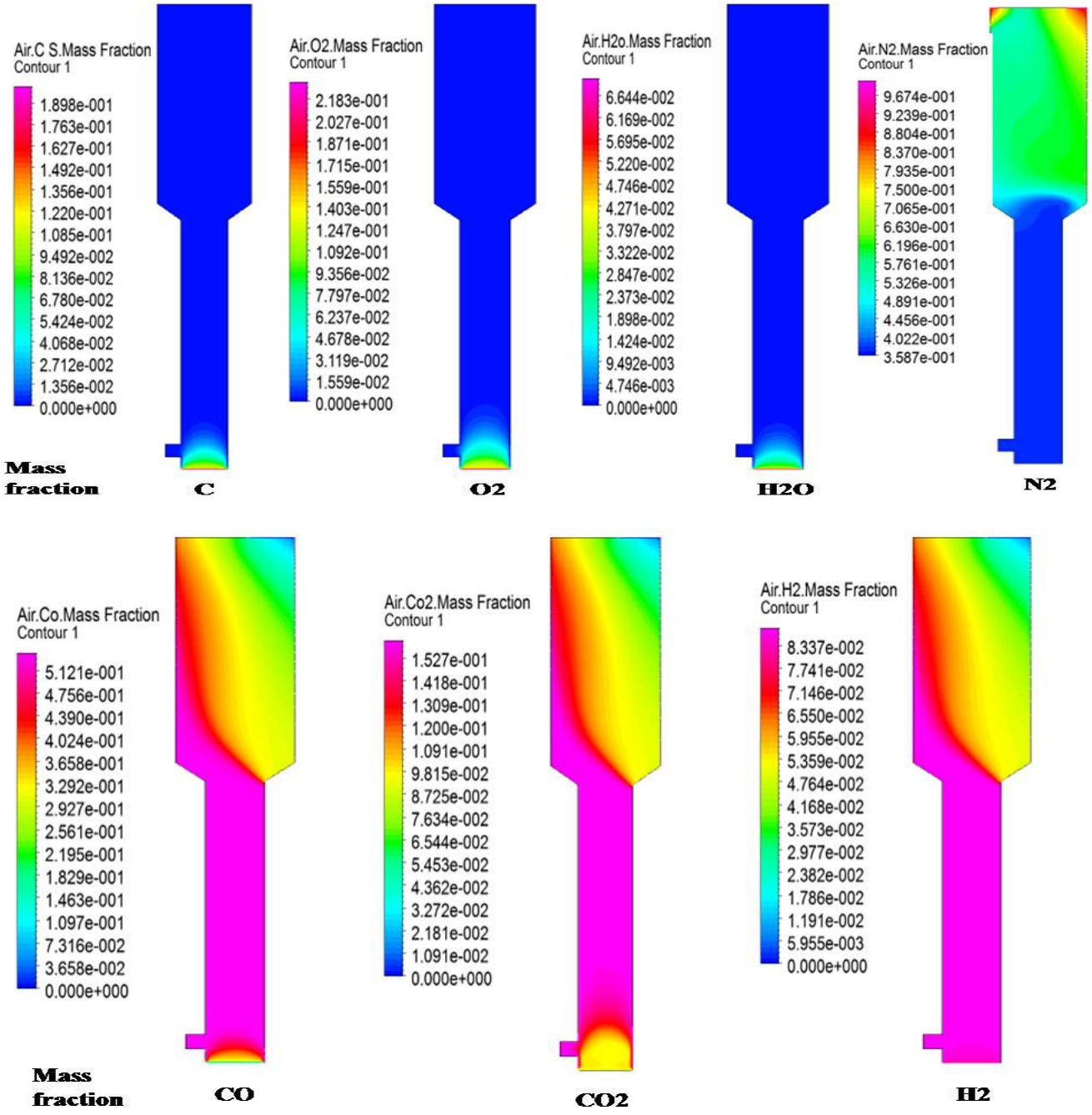

Fig. 6.4: Distribution of gas mass fractions

The gas species are observed at steady state and their variations in axial directions are plotted throughout the reactor (Fig.6.5). The mass fractions vary with the vertical position because of the impact of chemical reactions. The stable mass fractions at the outlet region ensure that steady state is reached.

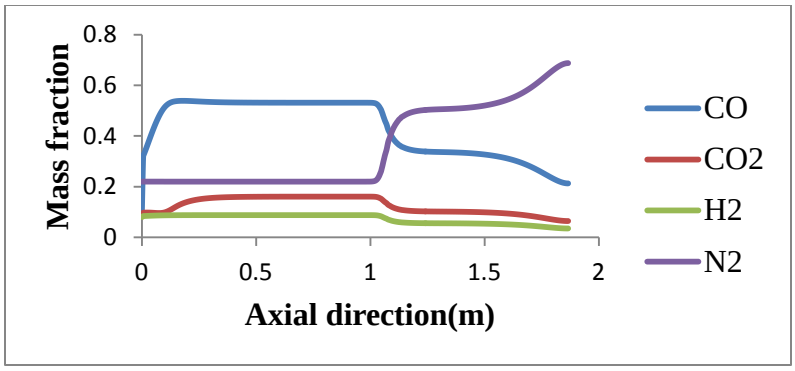

Fig. 6.5: Mass fractions at t=60s

The velocity vector colored by gas temperature in the geometry is illustrated in Fig. 6.6. The flow pattern inside the gasifier is complicated showing the flow field without the presence of particles.

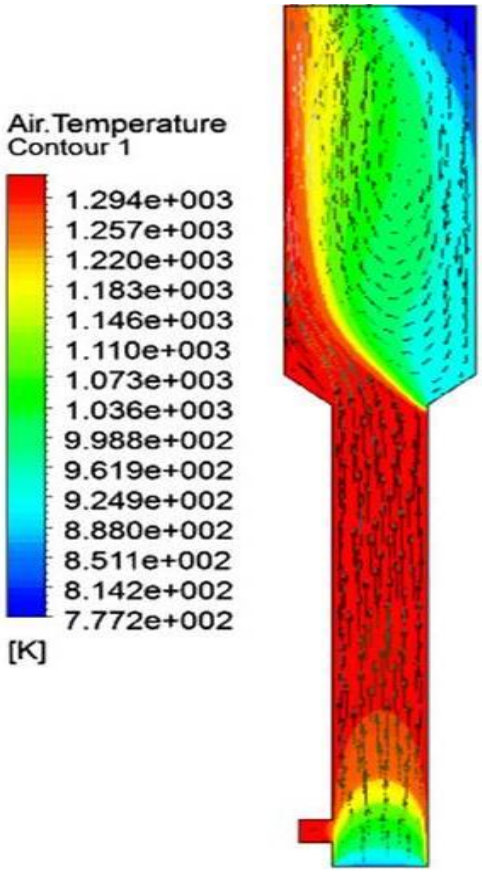

Fig. 6.6: Gas velocity vector plots coloured by temperature (K)

6.2.5 Variation in Temperature

The effect of bed temperature on the compositions of the exhaust gases is studied with models using four different temperatures such as 600,700,800,1000^{0}C. The average mass fractions of the gaseous species are shown in Fig. 6.7. Since gasification is an endothermic reaction, the product gas composition is sensitive towards temperature change. Results show that bed temperature has an important influence on the gasification process. Increase in the temperature increases CO and H_2 species. This further decreases CO_2 and H_2O species. This is because of the highly temperature dependent heterogeneous reactions. As the temperature increases the reactions take place faster leading to a faster consumption of the reactants, H_2O and CO_2 through the steam gasification reaction and Boudouard reaction, respectively. This subsequently leads to an increase in their products CO and H_2 which is apparent in Fig. 6.7.

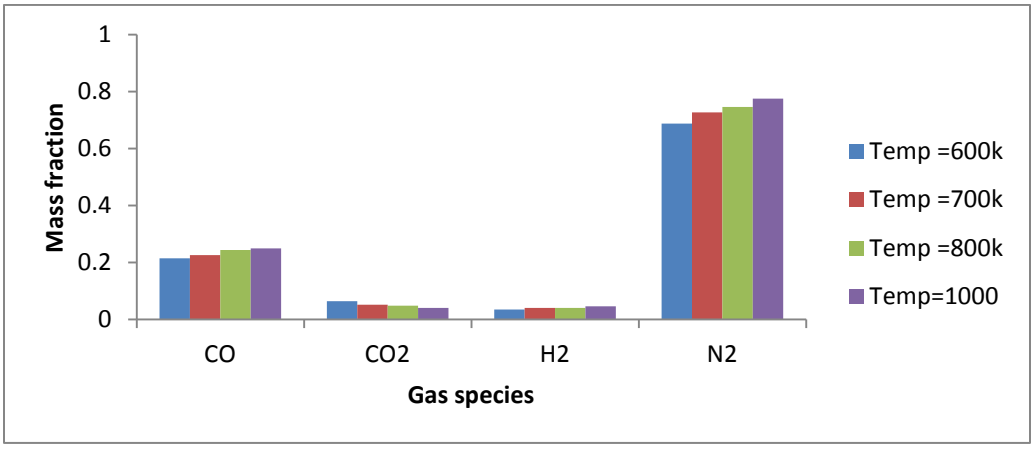

Fig. 6.7: The average mass fraction of each gaseous product through the outlet for varying temperatures

6.3 Case 3: Heterogeneous (Gas-solid) Reaction with Volatiles

Biomass gasification is a multiphase problem between gases and rice husk particles. It is also a reactive flow that involves homogeneous reactions among gases and heterogeneous reactions between ricehusk particles and gases. In this study, both gas phase (primary phase) and solid phases (secondary phases) are solved by using Eulerian multiphase model. Both homogeneous (gas-gas) reaction and heterogeneous (gas-solid) reactions are simulated in this case.

6.3.1 Phases and Materials

The case is simulated using three phases which enter the gasifier through boundary conditions and interact exchanging mass, momentum, temperature and species. These three phases are:

1. Gas phase (Primary phase): The gas phase is used for simulating both the steam inlet and the product gas outlet. This is achieved by including all the working species in one phase so that the mass and momentum equations are solved once per time step. It consists of O_2, N_2, H_2O, H_2, CO, CO_2 and CH_4. The properties of the species are taken from Ansys Fluent database. The gasifying agent is air considered at a constant velocity.
2. Solid (Secondary phase): This phase represents the fluidizing bed material, which is sand in this study. The sand is modelled as granular and inert material.
3. Solid (secondary phase): This phase simulates the fuel inlet of the gasifier. Rice husk is considered as the feed material in this study. It is considered to be a granular phase. It consists of solid carbon (C) representing char, H_2O for the fuel's moisture and CH_4 for the volatile matter.

Summary of used parameters with the name of models used in this study has been mentioned in table-5.2.

6.3.2 Boundary Conditions

At the inlet, velocity of air with a temperature is considered. Rice husk is entered through the left side of the reactor with velocity. The species mass fractions are determined from the proximate analysis of the rice husk. At outlet, outflow boundary condition is specified. In case of wall, no slip boundary condition is used for solid and fluid phase.

Table 6.4: List of principal boundary conditions

Property	Value	unit
Gas density(air)	1.2	kg/m^3
Gas viscosity	$1.7894*10^{-5}$	Pa.s
Rice husk density	426	kg/m^3
Ricehusk particle diameter	530	μm
Density of inert solid(sand)	2650	kg/m^3
Diameter of sand	385	μm

Superficial gas velocity	0.7	m/s
Static bed height of sand	0.05	m
Rice husk inlet velocity	0.005	m/s
Restitution coefficient, e	0.9	-
Temperature of air	673	k

Table 6.5: List of specific boundary conditions for different phases

Species mass fractions	Ricehusk(solid phase)	Air(gas phase)
H2O	0.0734	
C(s)	0.2046	
CH4	0.564	
O2		0.23
N2		0.77

6.3.3 System Kinetics

The model's accuracy strongly depends on the chemical reactions chosen and the reaction rates which determine the final product gas composition. The main effects of the gas phase conversion process and the solid phase gasification are given by the following reactions. Rate constants are given in the form of the Arrhenius equation:

$$K = A.\exp(E/RT) \quad (6.6)$$

In this equation, A is the pre-exponential factor which determines the speed of reaction while E is the activation energy and R is the ideal gas constant (R = 8:314kJ/kgK).

6.3.4 Solution Techniques

In Fluent, solver is set as segregated which solves the equation individually. Here pressure based solver is used. Species transport model is used. Eulerian multi-fluid model is adopted where gas and solid phases are all treated as continua, inter- penetrating and interacting with each other everywhere in the computational domain. The finite rate model is considered. Finite rate model is used to predict the reaction rate. The discretization scheme for momentum, energy and species all has been taken as second order upwind. For volume fraction of solid and gas phase Quick scheme is used. The under relaxation factors as mentioned in table 6.2 have

been used for different flow quantities. The convergence criterion for continuity, velocity and species has been taken as 0.001.

6.3.5 Results and Discussion

6.3.5.1 Phase dynamics

A brief analysis of the gas-solid dynamics in the bed is considered before the effects of the reaction kinetics are studied:

Fig. 6.8 shows snapshots of the gas void fraction from the beginning of the simulation where bubbles start to evolve and rise through the reactor. Rice husk is fed from the left just above the static bed height of sand. There are a number of observations that can be checked including the formation of bubbles along the left side of the reactor, formation of bubbles in the lower region of the bed and also its the variations along the bed height. The formation of bubbles up to the left wall is due to the buildup of gaseous products. This has taken place near the fuel inlet on the left hand side of the reactor after devolatilisation. As the gases build up, the bubbles increase in size and continue to rise up through the bed. The formation of larger bubbles near the top of the bed is a result of the coalescence of smaller bubbles. It is due to the movement of these bubbles through the bed that mixing is enhanced within a bubbling fluidised bed. The bubbles formed in the lower section of the bed are small in comparison to those observed at the upper section of the bed. At the inlet the oxygen concentration is highest and combustion takes place immediately on contact with the char particles in the bed. The gases form small bubbles that continue up the bed by increasing in size as further reactions and coalescence of bubbles take place.

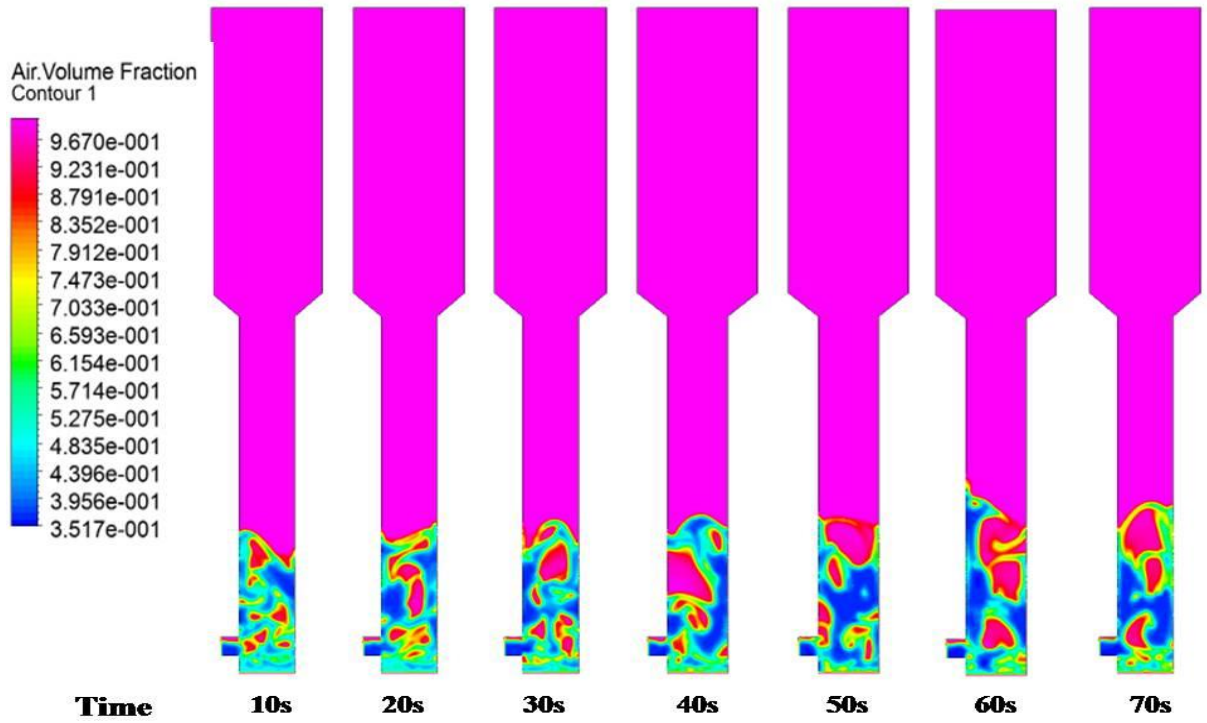

Fig. 6.8: Gas phase volume fractions at different time

The volume fraction of the ricehusk and sand are shown in Fig. 6.9 respectively. The lower density particles namely ricehusk, are segregating to the top of the bed. The figure shows a collection of sand towards the base of the bed while the ricehusk phase slightly dominates the centre and the top region of the bed. The sand having a higher density than the rice husk which would result in its settlement at the base of the bed whereas the smaller char particles segregate to the top of the bed.

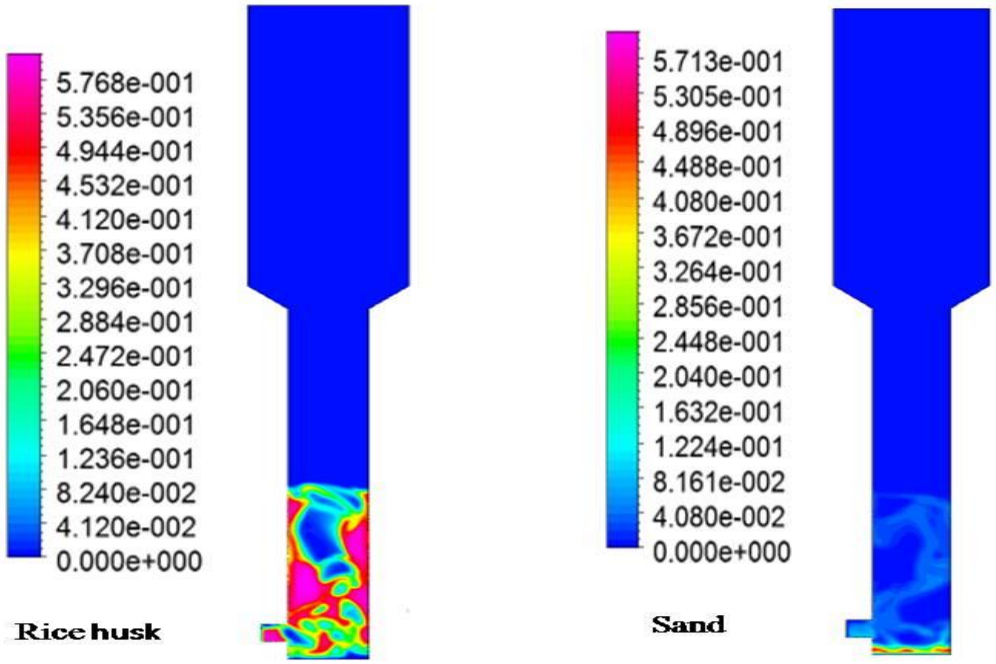

Fig. 6.9: Solid phase volume fractions

6.3.5.2 Gas Compositions

The gaseous mass fraction distributions within the reactor are given in Fig. 6.10. There is a clear distinction between the species introduced through the gaseous inlet and combustion process as these are more concentrated towards the base of the reactor compared to those which increase in concentration with increasing height. The region near the fuel inlet shows a particularly concentrated region for the gaseous species of CO, H_2 and CH_4. This region signifies the accumulation of devolatilisation products as the fuel is introduced to the bed at this point. The products then mix through the bed along with the products of heterogeneous reactions from the lower bed region to continually trigger further reactions, i.e., heterogeneously within the bed as seen in Fig. 6.10 and finally with the water-gas shift reaction which dominates over the bed.

It is apparent that the heterogeneous reactions result in a strong variation in the mass fractions within the bed. This is because the reactions depend on the local concentrations of the species which consequently influence further reactions as increased concentrations of their products accumulate.

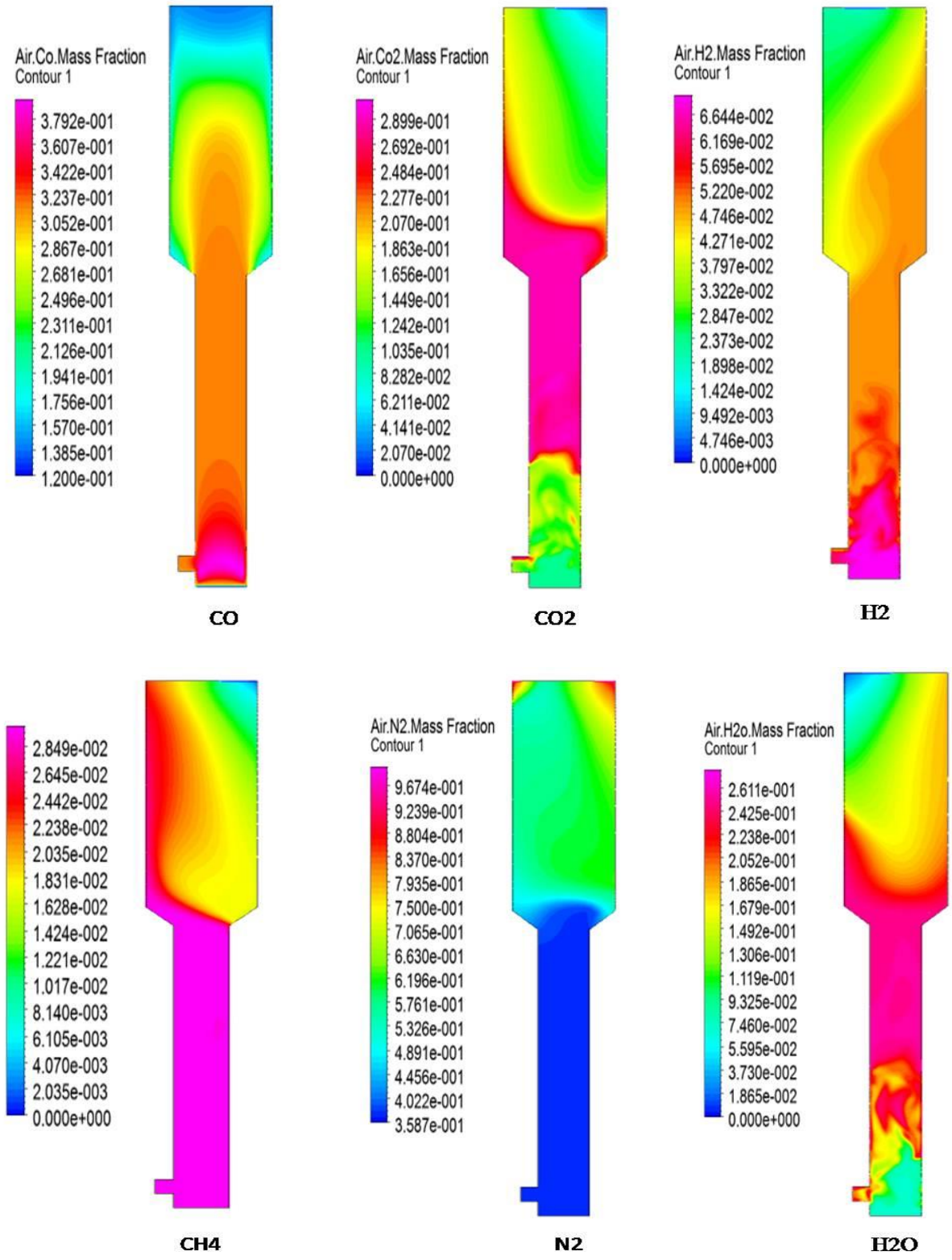

Fig. 6.10: Contour plot of distribution of mass fractions

6.3.5.3 Temperature Distributions

The Fig. 6.11 displays the contour plots of the gaseous temperature distribution for model. It is clear that the highest temperature is observed at the base of the reactor where the exothermic combustion reaction dominates. The variation in temperature throughout the bed is mainly depending on position and local reactions.

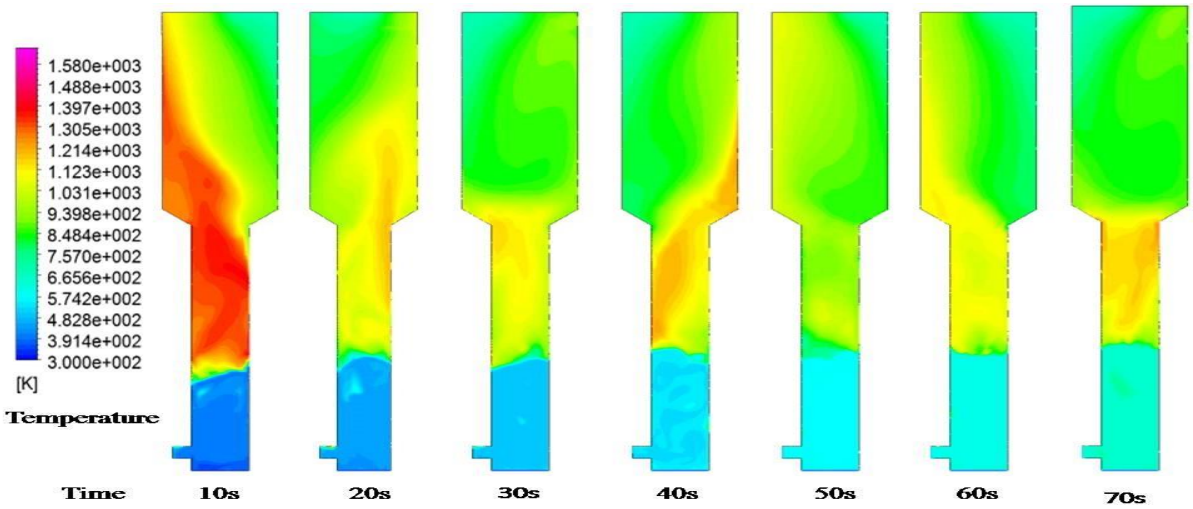

Fig. 6.11: Temperature distribution at different time inside the fluidized bed

Finally, the simulation results are compared to the actual experimental data (Fig.6.12). It is noticeable that N_2 and CO_2 are overestimated, while H_2 is underestimated. The CO and CH_4 mass fractions show acceptable agreement with the experimental data taken from co-researcher.

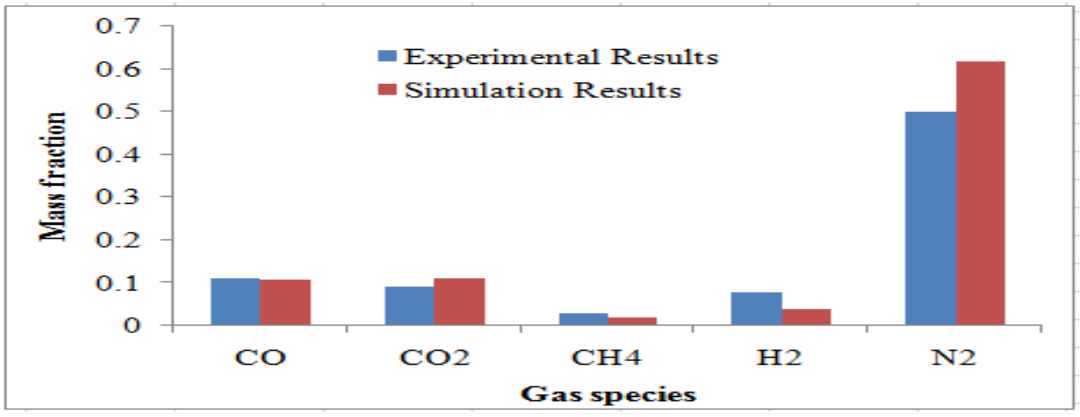

Fig. 6.12: Outlet results

CHAPTER SEVEN

CONCLUSION

CONCLUSION

In this study, CFD modelling of fluidized bed biomass gasifier has been conducted to get an innovative clean biomass gasification technology by using the commercial CFD solver ANSYS/FLUENT. The results yield comprehensive information concerning the thermal-flow behaviour and gasification process existing inside the specially designed fluidized-bed gasifier. Based on the results obtained in the simulation from this study, the following conclusions are drawn.

Hydrodynamic study

- Increasing superficial gas velocity makes the flow development faster implying that the superficial gas velocity has a strong influence on the axial solids velocity and subsequently on the down flow of solids.
- The bed expansion behavior is found to vary with variation in gas velocity.
- Solid inlet configuration significantly affects the distribution of the gas and solid volume fraction.
- Model is able to describe quantitatively the accumulation of solid at the wall. Solid concentrations appear flat in the core and increase towards the wall region.
- Back-mixing behavior or accumulation of particles has been perfectly exist in the FB, since the velocity in the core region are upward flow and much higher than that in the annulus region, while solid and gas velocities near wall are decreasing.
- The CFD simulation exhibited a solid circulation pattern for all the operating conditions which is observed to be consistent with the literatures reported by various investigators.
- The velocities of the smaller particles are larger than that of the biger particles in the lower zone due to the attainment of high slip on the bottom side. The volume fraction of big particles is lower in the upper region than that in the lower portion of the riser.
- The simulation models achieved in predicting the bed dynamics of the fluidized bed reactor such as its temperature and pressure distribution are also found to be satisfactory.

Reaction Modelling

- Bubbles are formed both exogenously and endogenously as a result of the reaction kinetics. Multiple phases for the bed phases, rice husk and sand, led to phase segregation

as lower density rice husk particles migrated towards the top of the bed and the denser sand particles descended to the base of the reactor.

- Both instantaneous (homogeneous reaction) and finite-rate (heterogeneous reaction) gasification models are used in the simulation. The results show that the heterogeneous model predicts the temperature and species concentration reasonably well. The instantaneous gasification model over-predicts reaction rates. Gas temperature and species distributions indicate that reactions in the instantaneous gasification model occur very fast and finish very quickly with a indicating 100% carbon conversion. On the other hand the reactions in the finite-rate model involves gas-solid reactions, occur slowly with unburnt chars at the exit.
- The mass fractions of product gas are also validated with the experimental data.
- Increasing bed temperature led to an increase in the highly temperature dependant heterogeneous reaction rates further leading to an increase in the reaction products and decrease in their reactants.

REFERENCES

.1. "ANSYS FLUENT 12.0", Theory Guide, 2009.

2. "ANSYS FLUENT 12.0", User's Guide, 2009.

3. Baosheng J., Xiaofang W., Wenqi Z., "Modeling on high-flux circulating fluidized bed with Geldart group B particles by kinetic theory of granular flow", Energy Fuels, 24, 3159 – 3172, 2010.

4. Basu P., "Combustion and Gasification in fluidized bed", CRC Press, Taylor & Francis Group, New York, 2006.

5. Dimitrios, S., "Investigation of biomass gasification conditions for energy production", General Secretariat for Research & Technology of Greece, Joint Research &Technology Programmes, Greece-Slovakia, Final Report, 2001.

6. Faeth, G.M., "Mixing, transport and combustion in sprays", Progress in Energy Combustion Science, 13, 293 - 345, 1987.

7. Fletcher, D. F., Haynes, B. S., Christo, F. C., Joseph, S. D., "A CFD based combustion model of an entrained flow biomass gasifier", Applied Mathematical Modelling, 24(3), 165- 182, 2000.

8. Gerun L., Paraschiv M., Vijeu R., Bellettre J., Tazerout M., Gøbel B., Henriksen U., "Numerical investigation of the partial oxidation in a two-stage downdraft gasifier" Fuel, 87, 1383 – 1393, 2008.

9. Gidaspow D., Bezburuah R., Ding J., "Hydrodynamics of circulating fluidized beds: Kinetic theory approach",In Proceedings of the 7th Fluidization Conference,75-82,1992.

10. Gidaspow D., "Multiphase flow and fluidization, continuum and kinetic theory Descriptions", Academic Press, Inc., 1994.

11. Hamzehei M., Rahimzadeh H., Ahmadi G., "Studies of gas velocity and particles size effects on fluidized bed hydrodynamics with CFD modeling and experimental investigation", Journal of Mechanics; 26(3), 2010.

12. Huiyan Zhang, Shanshan Shao, Rui Xiao, Qiwen Pan, Ran Chen, Jubing Zhang, "Numerical study on the hydrodynamics of a self-heating biomass fast pyrolysis reactor" Energy Fuels, 25, 4077 – 4084, 2011.

13. Kunii D. and Levenspiel O., "Fluidization Engineering", Second Ed., Butterworth Heinemann, Boston, 1991.

14. K. Papadikis and gu, "CFD modelling of the fast pyrolysis of biomass in fluidized bed reactors", Part A: Eulerian computation of momentum transport in bubbling fluidized beds", Chemical Engineering Science, 63, 4218 - 4227, 2008.

15. Kumar A., Kent E., David, D. Jones. , Milford, A. Hanna. , "Steam–Air fluidized bed gasification of distillers grains: effects of steam to biomass ratio, equivalence ratio and gasification temperature", Bio resource Technology, 100, 2062 – 2068, 2009.

16. Lendon T.R., Mc Lui A. P., Pineault R.L., Beer S.K., Richardson S.W., "High pressure co-gasification of coal and biomass in a fluidized bed", Biomass and Bio energy, 26, 377-388, 2004.

17. Liang Y., Xiangping Z., Suojiang Z., "Numerical simulation of the bubbling fluidized bed coal gasification by the kinetic theory of granular flow (KTGF)", Fuel, 86, 722 - 734, 2007.

18. Lun C.K.K, Savage, S.B. Jeffrey, D.J. and Chepurniy, N., "Kinetic Theories for Granular Flow: inelastic particles in couette flow and slightly inelastic particles in a general flow field", Journal of Fluid Mechanics, vol.140, pp 223-256, 1984.

19. Patankar, S.V., "Numerical Heat Transfer and Fluid Flow", McGraw-Hill, New York,

1980.

20. Peng B., Zhu J. Zhang C., "A new approach to specify the inlet boundary conditions for computational fluid dynamics (CFD) modeling of hydrodynamic behavior of a circulating fluidized bed (CFB) riser", Ind. Eng. Chem. Res., 51, 2152 – 2165, 2012.
21. S. Gerber, M. Oevermann, "An Eulerian modeling approach of wood gasification in a bubbling fluidized bed reactor using char as bed material", Fuel, 89, 2903-2917, 2010.
22. Syamlal, M. "The particle-particle drag term in a multi particle model of fluidization", In National Technical Information Service, Springfield, VA, 1987.
23. Taghipour F., Ellis N., Wong C., "Experimental and computational study of gas–solid fluidized bed hydrodynamics", Chemical Engineering Science, 60, 6857 – 6867, 2005.
24. Tingwen L., Aytekin G., Madhava S., "High-Resolution simulations of coal injection in a gasifier", Ind. Eng. Chem. Res., 49, 10767–10779, 2010.
25. Wang Y., Yan L., "CFD studies on biomass thermo chemical conversion", Int J Mol Sci, 9, 1108 – 1130, 2008.
26. Wen Y.C., Yu. Y.H., "Mechanics of fluidization", Chem. Eng. Prog. Symp. Ser., 62:100, 1966.
27. Yiqun W., Lifeng Y., "CFD modeling of a fluidized bed sewage sludge gasifier for syngas", Asia-Pac. J. Chem. Eng., 3, 161 – 170, 2008.
28. Yanping L., Bingjie M., Jinbang H. K. Z., Numerical simulation of the hydrodynamics of gas/solid two-phase flow in a circulating fluidized bed with different inlet configurations", Research Article, Chem. Eng. Technol., 32, 6964–6970, 2009.
29. Zhou M., Yan L., Guo Q., "Non premixed combustion model of fluidized bed biomass gasifier for hydrogen rich gas", Chinese Journal of Chemical Physics, 19, 2006.